EFFECTS OF PRIOR AGING AT 191°C ON CREEP RESPONSE OF IM7/BMI 5250-4

THESIS

Robert A. Salvia, LCDR, USN

AFIT/GAE/ENY/07-J23

DEPARTMENT OF THE AIR FORCE
AIR UNIVERSITY

AIR FORCE INSTITUTE OF TECHNOLOGY

Wright-Patterson Air Force Base, Ohio

The views expressed in this thesis are those of the author and do not reflect the official policy or position of the United States Navy, United States Air Force, Department of Defense, or the U.S. Government.

AFIT/GAE/ENY/07-J23

EFFECTS OF PRIOR AGING AT 191°C ON CREEP RESPONSE OF IM7/BMI 5250-4

THESIS

Presented to the Faculty

Department of Aeronautics and Astronautics

Graduate School of Engineering and Management

Air Force Institute of Technology

Air University

Air Education and Training Command

In Partial Fulfillment of the Requirements for the

Degree of Master of Science in Aeronautical Engineering

Robert A. Salvia, BSAE

LCDR, USN

June 2007

AFIT/GAE/ENY/07-J23

EFFECTS OF PRIOR AGING AT 191°C ON CREEP RESPONSE OF IM7/BMI 5250-4

Robert A. Salvia, BSAE

LCDR, USN

Approved:

_____//SIGNED//_____	_____
Dr. Marina Ruggles-Wrenn (Chairman)	Date
_____//SIGNED//_____	_____
Dr. Richard B. Hall	Date
_____//SIGNED//_____	_____
Dr. Som Soni	Date

Abstract

The creep behavior of IM7/BMI 5250-4 with fiber orientations of [±45] and [0/90] that were aged in air at 191ºC for up to 1000 hours was evaluated. The total weight loss during the aging process was also evaluated. Weight loss due to aging was 0.64% for the [0/90] fiber orientation and 0.72% for the [±45] fiber orientation.

Tensile tests to failure were conducted to establish tensile properties. The [0/90] specimens have a much higher stiffness and Ultimate Tensile Strength (UTS) values than the [±45] specimens. The tensile tests of the aged specimens revealed that the Ultimate Tensile Strength of the composite decreased and the modulus increased with increasing prior aging time.

Creep tests were conducted at 191ºC. The creep tests were of 100 hour duration and were followed by unloading to zero stress and 60 hours of recovery at zero stress.

Acknowledgments

There were many people who without their assistance I could not have completed this study and who I have to thank; Dr. Marina Ruggles-Wrenn for her constant help and guidance throughout the entire process and for providing countless articles and resources; Dr. Greg Schoeppner, Dr. Charles Y-C Lee, and Dr. Richard Hall for their sponsorship of this study and their continued support. Dr. Bill Ragland for assisting in the aging process of the specimen; Ron Trejo for his detailed information about the manufacturing of the material; Barry Page, Jay Anderson and Sean Miller for keeping all of the systems and machines working through power outages and other events to keep the data coming.

I would also like to thank my parents for always stressing the importance of education, my wife for suffering through the countless nights of being an “AFIT widow” and finally my son who reminded me everyday on the way to kindergarten that school is really fun.

Robert A. Salvia
LCDR USN

Table of Contents

Page

Page

List of Figures

Figure **Page**

Page

Page

Page

Page

List of Tables

Table **Page**

EFFECTS OF PRIOR AGING AT 191°C ON CREEP RESPONSE OF IM7/BMI 5250-4

I. Introduction

Composite materials are not new. Ever since humans have been building things they have been looking for better and stronger materials to build with. They began using composites “centuries ago when humans were making dwellings from mud and straw”.(8:4) The reinforcement of cement with steel bars dates back to the nineteenth century when masonry was reinforced with iron bars.(20:2) From these beginnings came the understanding of how to improve the mechanical properties of building materials. These advances were strictly to improve the strength of building materials; there was no concern about limiting the weight of the material at that time because these were for land based structures. However, that all changed with the birth of aviation.

Since the beginning of aviation engineers have been searching for ways to build stronger and lighter aircraft. As early as 1933 aeronautical engineers realized that in “aeronautics the weight of every part has to be reduced to the absolute minimum compatible with safety.”(5:1) Axial tensile testing was being conducted back then on the

metals, fabrics, timber and rubber that was being used to build aircraft. These tests are still being done today on much more sophisticated materials, which can be manufactured to display specific strengths for very specific uses

The ability to manufacture composites with tailored strength properties is one of the main advantages over metals. Metals have a uniform strength in all directions, this may be necessary for some applications. However if a piece of equipment is only going to be subjected to one type of load a composite can be designed to handle that specific load while at the same time reducing the overall weight of the equipment.

Aviation has been the driving force behind composites. As early as the 1960s, commercial aircraft were using glass-reinforced composites for secondary structures. During the 1970s the availability of carbon fibers and the rising fuel costs led to rapid development of structural composites for airframe applications due to their increased strength but more importantly for the decrease in weight. It was in the early 1980s that carbon based composites were first used on a production scale for the generation of aircraft that included Boeing 757, 767 and others. (7:36) Composites were still only being used on secondary structures at this time.

It is easy to see the advantages of composite materials in aerospace applications, there are some disadvantages that have slowed the growth until recently. The main factors holding back the growth of composites were strength and cost. With all of the advantages composites add to aerospace design there has been a large push in designing new matrix materials and reinforcing fibers that are stronger and can be tailored to specific needs. Also there is a large push to design composite materials that can retain these properties in higher temperatures. Bismaleimide (BMI) resins with carbon reinforcing fibers are

currently being used most extensively in aerospace applications because of their strength and workability. They are however limited in their use because of the temperature limitations.

Cost is not only limited to the cost of acquiring the materials but also the cost of repairing the materials once they are used in aircraft construction. This contributes to the lifetime cost of materials. Metals are heavier but they are cheaper to acquire and cheaper to repair. Composites are getting easier to repair but the cost is still higher. As the percentage of the aircraft that can be made out of composites increases, the savings in production and fuel will overcome the higher cost of composites.

The lighter weight and increased strength of composites and the ability to mold polymers into various shapes have put polymer composites at the leading edge of aerospace design. The direction that aeronautical design is heading has now been clearly defined. As composites continue to develop increased temperature resistance, and strength, they will have even greater presence in advancing aerospace designs. As aviation designers look forward to unmanned air vehicles for the military, composites are figured to play an even larger role. These aircraft are being designed to withstand 2 or 3 times the current g-force requirements to perform evasive maneuvers to avoid enemy missiles. These aircraft will have to be all-composite construction to achieve these performance factors. (33:442)

II. Background

This section presents the basic definition of composite materials including polymers and carbon fibers, and the advantages of composites over other solids. This section will also address previous work that has been done on similar polymers and the objectives of this thesis will be defined.

Composites

A basic definition of a composite means “made of two or more different parts” that when combined they form a “material of which the set of performance characteristics is greater than that of the components taken separately. (6:3) One of the materials is the matrix and the other material is the reinforcing portion of the composite. The matrix is referred to as the continuous phase and it binds together the reinforcing material which is usually a harder material and has superior mechanical properties than the matrix. (6:3)

Composites can be divided into two large classes according to the type of reinforcement used. There are composites with fiber reinforcement and there are composites with particle reinforcement. Particle composites are generally used to improve the certain properties of materials such as stiffness or behavior at temperature. An example of a particle composite would be lead inclusions in copper alloys to make them easier to machine. (6:6)

Fiber composites use fibers to reinforce the matrix. The fibers can either be non-continuous or continuous. The orientation of the fibers in the matrix allow for the mechanical properties of the composite to be tailored for specific loads and uses. Fiber composites can be further divided by the type of matrix that is used. There are Organic

matrix composites that consist of polymer resins, metallic matrix composites that use metal alloys as the matrix, and there are mineral matrix composites that use ceramic as the matrix. Each of these composites is suited to work in different temperatures. Organics are generally used below 300ºC while metals can operate up to 600ºC and Ceramics can operate up to 1000ºC.(6:7)

Composites can also use many different fibers as reinforcement. The two most commonly used fibers are glass and carbon. Advantages of glass fibers include low cost and high tensile strength as well as excellent insulating properties. Disadvantages of glass include low tensile modulus, and low fatigue resistance. Glass fibers are the most commonly used fiber for all polymeric matrix composites (PMC). Carbon Fibers have exceptionally high tensile strength to weight ratios and high fatigue strengths. They also have a very low thermal expansion coefficient. The main disadvantage to carbon fibers is that they are very expensive compared to glass fibers. Because of this high cost carbon fibers are predominantly used in the aerospace industry where lowering weight is more important than cost. (19:22-29) The application of the composite is what ultimately determines the materials that are used.

The mechanical properties of a composite depend on the materials that make up the matrix and the reinforcing fibers. But it is also heavily dependent on the orientation of the fibers as well as the volume fraction of fiber (V_f) The higher percentage of fiber in the composite will lead to a higher strength and performance. The orientation of the fibers will also have a large effect on the properties. The more non uniform the distribution of fibers, the more heterogeneous the material is, resulting in a higher probability that the material will fail in the weaker areas.(20:2) By determining what type of load the

composite will have to bear, it can be tailored to meet the desired specification through the orientation of and volume fraction of fibers. In the case of low to medium performance composite materials, short fibers or particles are often used to enhance stiffening but only provide limited strengthening of the material. In these instances the matrix is the main load bearing part of the composite and has the largest effect on the mechanical properties. In the case of high performance composites, continuous fibers are used and the fibers determine the stiffness and the strength of the material in the fiber direction. The matrix provides protection for the fibers and helps transfer the stress from one fiber to another. (20:2)

Polymers

Polymers exist in nature and they can be man-made as well. All polymers, whether organic or inorganic, consist of extremely large molecules, called macromolecules, in which the atoms in the polymer chain are held together by covalent bonds. (13:1) The most common natural polymer is rubber. There is evidence that as early as 1500 Mayans were using rubber in their everyday lives. In 1839, Charles Goodyear discovered vulcanization, the adding of sulfur to natural rubber and heating it up to 270^{o} F. (9:54) this process led to a polymer substance that was much more durable than natural rubber alone.

The oldest known synthetic resin was first introduced in 1927 and was used for electric insulation. From this beginning chemical companies began research and development resulting in the first commercially successful synthetic rubber in 1932. (9:67) Today polymers are the most used material in the Unites States per unit volume.

We use more plastic then steel, aluminum and copper combined. Advanced composite theory has been at the forefront of technology since the 1950's and 60's.

Polymers are commonly classified into 3 groups: elastomers, thermoplastics, and thermosets. Thermoplastics are often divided even further into either crystalline or amorphous. (14:6) Figure 2 illustrates the different classifications of polymers and gives examples of each type.

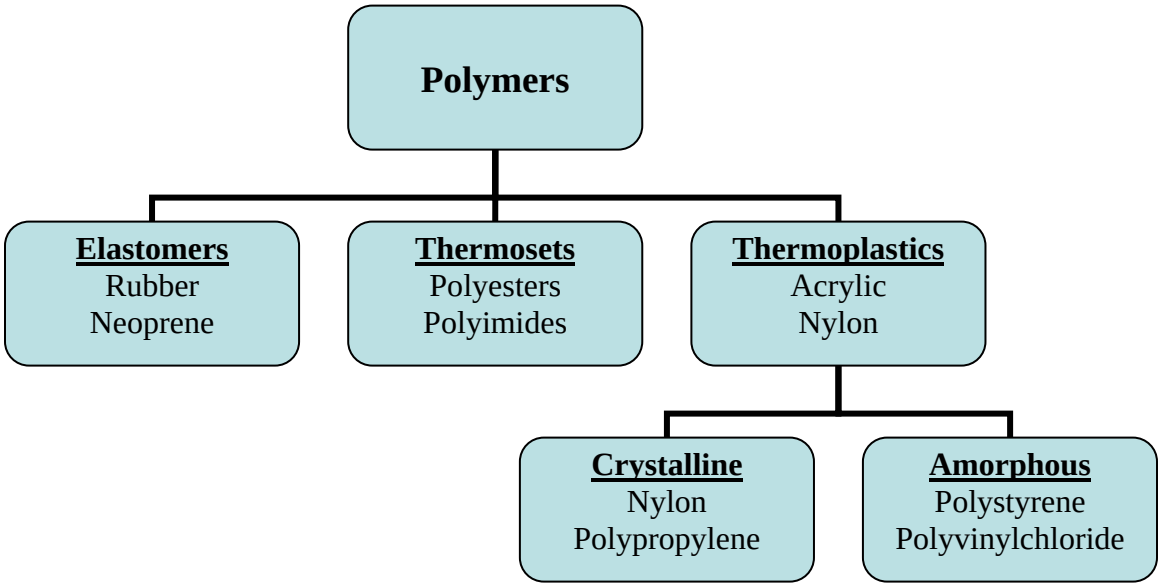

Figure 2: Classifications of Polymers

The defining characteristic of elastomers is the ability to be "easily deformed, reaching extensions of up to ten times their original dimensions and rapidly recovering their original size when the tension is released."(14:6) Natural and synthetic rubbers are common elastomers. Thermoplastics and thermosets are referred to as "engineering plastics." They combine light weight and corrosion resistance with high stiffness and toughness over a wide temperature range. (16:5)

Thermoplastics become fluid when heat is applied. They can be molded into shapes through either injection molding or extrusion. “In both techniques the Thermoplastic is heated to the liquid state, formed to the required shape under an appropriate pressure, and then cooled to solidify.”(16:264) The heating and cooling process can be repeated for thermoplastics; however the mechanical properties are degraded each time. (18:1)

The difference between the amorphous and the crystalline thermoplastics is in how the molecules form together after cooling. When a thermoplastic in the liquid state is cooled crystallization may occur. Crystallization is when the resulting polymer is characterized by the presence of “ordered crystalline regions as well as amorphous regions”(1:50) Often times however this crystallization does not occur and the molecular chains remained disordered after cooling resulting in an amorphous polymer. The transition from a liquid to an amorphous solid occurs at a temperature referred to as the glass transition temperature (T_g). The glassy state of the polymer may be considered a “frozen in liquid state” (1:51) where the polymer is solid and rigid. Crystalline polymers differ from amorphous polymers in that they have a melting temperature (T_m) that is higher than the glass transition temperature for an amorphous polymer. The organized regions in the crystalline plastics are joined together by amorphous regions. Crystalline plastics are stronger and stiffer than amorphous plastics, though they are less impact resistant. (18:2)

The forming of thermosets is somewhat more complicated. Thermoset polymers must be heated to an appropriate temperature for a predetermined period of time. Once this temperature is reached the polymer flows like a viscous liquid. At this point a “slow

chemical cross-linking reaction then causes the liquid to solidify to form an infusible mass."(16:5) This entire process must be done inside a mold, so that after the heating process occurs the thermoset takes the shape of the mold. The thermoset is then cooled and removed from the mold. Thermosets cannot be transformed once their shape is obtained. They also do not flow when heated like thermoplastics, "instead they undergo degradation at high temperatures."(14:7)

While thermoplastics may be used more extensively in everyday items, thermosets are used primarily for high performance applications such as aerospace. This is due to the high glass transition temperature of thermosets, which is a result of the highly cross linked molecular structure of thermosets.

Carbon Fibers

Carbon Fibers were first used as light bulb filaments in 1879. Soon after around 1910, tungsten filaments were found to be superior to carbon fibers and this use of carbon fibers was abandoned. Other uses for carbon fibers were experimented with to include insulation, but nothing caught on. "It was not until the late 1950s that work carried out at Wright Patterson Air Force Base on developing high-strength carbon fibers that the industry saw an upsurge."(17:1) The research conducted resulted in the production of high-strength and high-modulus rayon based carbon fibers. At relatively the same time Japanese companies were perfecting a method of making polyacrylonitrille or (PAN) based carbon fibers. The third method of producing carbon fibers is the asphalt or pitch method.

Carbon Fibers are categorized both by the method in which they are made and by their mechanical properties. The specific process of manufacturing carbon fibers differs

for each of the three types of fibers. However there are some essential features that are similar. They involve “a stabilizing treatment to prevent melting or fusion of the fiber, a carbonizing heat treatment to eliminate the noncarbon elements, and a high temperature graphitizing treatment to enhance the mechanical properties of the final fiber.”(17:16)

The production of the rayon fibers requires that the fibers be stretched during the graphitizing process at a high temperature. This is the most expensive method of production and yields the least amount of fibers about 20-25%. This method has been largely phased out because of the lower production yields and generally poorer mechanical properties than fibers made from PAN or pitch.

The PAN method uses a multistage process to form carbon fibers. The process can modify the modulus of the final fiber by applying the graphite at different temperatures up to 3000ºC. Fibers produced by the PAN method have the advantages of being easily spun into highly oriented very fine fibers that are stable and have a relatively high yield.(8:205) PAN fibers are available with moduli ranging from medium (235GPa) to high (340 GPa) depending on the processing temperature.

The pitch fibers are also produced in a multistage process. The fibers are spun under stress at a low temperature to properly orient the fibers. “The pitch method produces highly oriented high-modulus carbon fibers without stress graphitization.” (17:16) This process produces fibers with a very high modulus without having to be stretched at high temperatures. “Fibers produced with this method have approached the theoretical value for a graphite crystal: 1000GPa” (8:206) The main advantage of producing fibers from pitch over PAN is that no tension is required to orient the fibers for high modulus and strength due to the molecular composition of the pitch. (8:66)

Carbon Fibers are also categorized by their general mechanical properties into three types; High Modulus (HM, Type I), High Strength (HS Type II), and Intermediate Modulus (IM, Type III). (33:6) Table 1 presents the different mechanical properties for the three general categories of carbon fiber.

Table 1: Properties for different types of Carbon Fibers

Property	**HM Type I**	**HS Type II**	**IM Type III**
Specific Gravity	1.9	1.8	1.8
Tensile Modulus (GPa)	276-380	228-241	196
Tensile Strength (MPa)	2415-2555	3105-4555	4800
Ultimate Strain (%)	0.6-0.7	1.3-1.8	2.0

The ability to mass produce carbon fibers with high-strength and high-modulus has greatly increased its use in all aspects of industry and design. Today, Nearly 8 million pounds of carbon fibers are produced each year. (10:342) The advantages that carbon fibers add to a polymeric composite are the following properties. Carbon fibers are extremely low weight. They are second only to organic fibers such as Kevlar in being the lowest density structural fiber. Carbon fibers have a very high stiffness. On a weight specific basis, the modulus of carbon fiber is nearly five times that of steel. Table 2 shows the mechanical properties of ultra high and high modulus carbon fiber compared to C-35 steel and 6061-T6 Aluminum alloy. This table clearly shows the advantages of carbon fiber to these other materials. Carbon Fibers are very stable at high temperatures. Carbon fibers have a small, negative coefficient of thermal expansion at all temperatures below 375ºC. This property along with their high modulus allows materials to be

designed with a near-zero thermal expansion when combined with different matrices. (10:348-349)

Table 2: Comparison of properties of Carbon, steel and aluminum

Material	Modulus (GPa)	Tensile Strength (MPa)	Density (g/cm^3)	Specific Modulus (GPa)	Specific Strength (MPa)
Carbon UHM	483	2270	2	281.5	1135
Carbon HM	345	2530	1.8	191.6	1405
Steel	206	420	7.8	26.4	54
Aluminum	69	260	2.56	27	101

Viscoelastic Behavior

Materials can be roughly categorized into two different types; viscous liquids and elastic solids. The best way to characterize between these two responses is how they react to a suddenly applied stress that is held constant thereafter. Liquids are referred to as viscous because when a sudden force is applied the liquid will deform in shape dissipate all of the energy as heat and not return to its original shape, rather it will be in steady flow. Elastic solids on the other hand will maintain a constant deformation when a load is applied. (22:1) For example metals will deform to a finite amount in relation to the load applied and will hold there until the load is removed. Below the yield point, metals will exhibit what is called linear elastic behavior. That is that an increase in stress will correspond with an increase in strain. If the load is removed the material will return to its original shape.

Polymers and polymeric composites fall into a category that is between a viscous liquid and an elastic solid and they are referred to as viscoelastic. What defines polymers as being viscoelastic is that they will exhibit the properties of both solids and liquids at different times and different temperatures. For example a polymer does not maintain a constant deformation under constant stress, instead it will continue to deform with time. This phenomenon is referred to as creep. If a viscoelastic polymer is held at a constant deformation, the stress required to hold it there diminishes or relaxes. This is an example of polymers acting in a viscous manner. Polymers also display elastic properties in that they do not dissipate all of the energy as heat. They will deform and continue to deform under constant stress. However if the load is removed polymers will recover part of its deformation.(21:2) The study of viscoelastic materials commonly involves tests for creep response, creep recovery, and relaxation.

Creep

Creep is a time-dependent deformation which occurs when a material is subjected to a load for a prolonged period of time. (24:1) As discussed earlier in a linearly elastic response a material will deform for a given load and hold there as long as the load remains constant. Creep describes the phenomenon where the material continues to deform even though the stress remains the same. A material cannot creep indefinitely and if allowed to continue creeping the material will eventually fail. That is why analyzing creep is important when analyzing materials.

Creep can be described in three parts. These are primary creep, secondary or steady state creep, and tertiary creep. A graph illustrating the different stages of creep is shown in Figure 3.

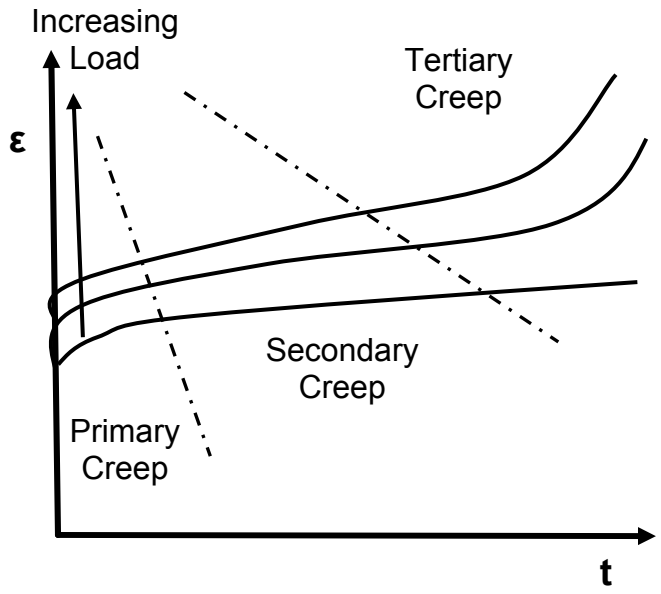

Figure 3: Schematic depicting the three stages of creep; Primary, Secondary and tertiary and how the curves are affected by an increase in load

Primary creep is defined as the portion of the curve where the creep strain rate is decreasing. Secondary or steady state creep is the portion of the creep strain curve where the creep rate is constant. Tertiary creep is where the creep strain rate increases, often rapidly, and is often followed quickly by failure. Note that not all materials will exhibit tertiary creep before failure.

Recovery

Once the stress is removed from the specimen, a reverse strain will occur followed by a recovery of a percentage of the creep strain that was occurred during

loading. The rate at which the strain is recovered will continue to decrease over time. Metals often show less creep strain recovery than do polymers. Some polymers may exhibit full recovery of the creep strain if they have enough time to recover. A graph of creep and recovery phase for pure elastic, pure viscous and viscoelastic material is shown in Figure 4.

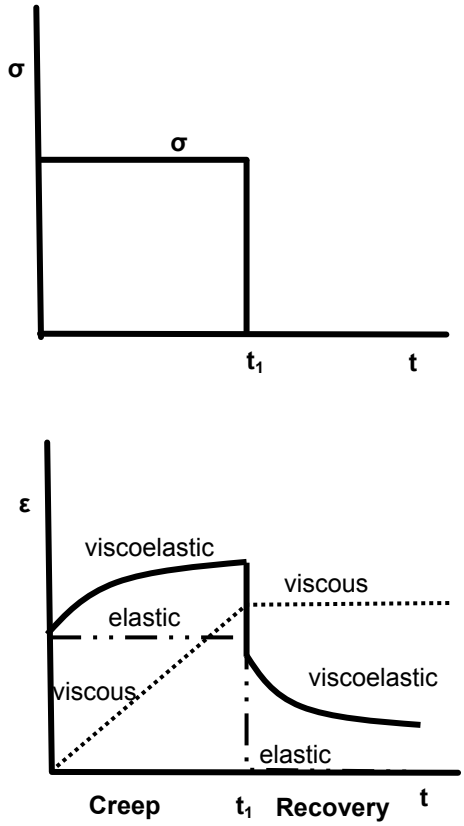

Figure 4: Schematic of creep and recovery depicting the behavior for viscous, elastic and viscoelastic materials that are subjected to a constant stress during the creep phase and unloaded to zero stress for recovery

Relaxation

Relaxation describes the viscous qualities of viscoelastic polymers. If a viscoelastic polymer is subjected to a constant strain, the stress required to maintain that strain will gradually decrease. Compare that to an elastic material and the stress will remain constant for a constant strain. A graphical representation of this is shown in Figure 5.

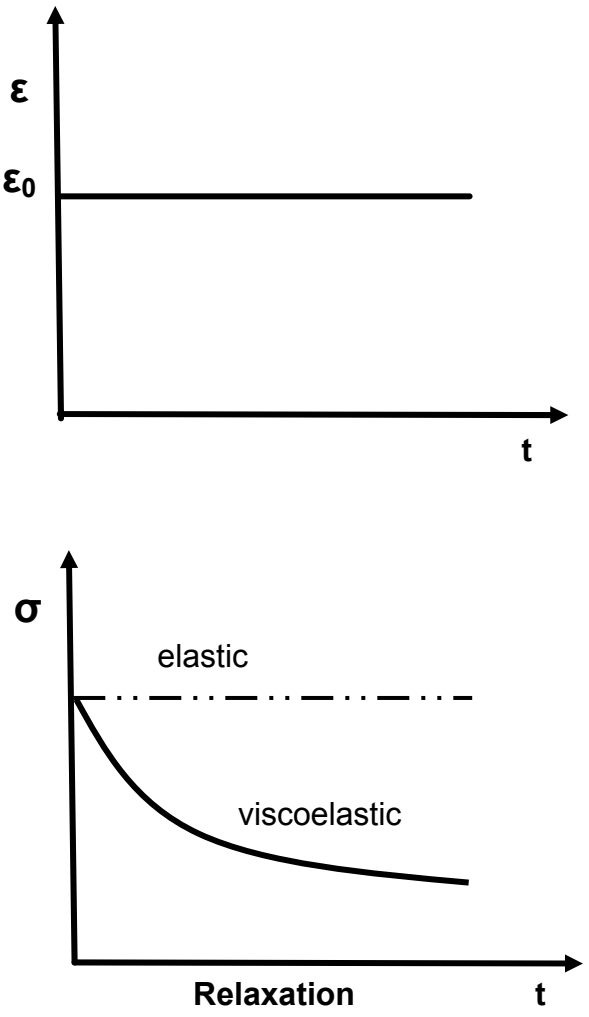

Figure 5: Schematic showing the stress behavior of elastic and viscoelastic materials during relaxation at constant strain

Linear Viscoelasticity

A material is considered linearly viscoelastic if stress is proportional to strain at any given time, and the Boltzmann superposition principle holds at all times.(23:5) The first requirement can be represented by the following equation

$$\varepsilon[c\sigma(t)] = c\varepsilon[\sigma(t)] \tag{1}$$

in which σ and ε are the stress input and strain output respectfully and c is a constant. The equation states that the strain-time output due to a stress input equals the constant c times the strain output due to a stress input.

The Boltzmann super position principle states that the sum of the strain outputs resulting from each component of stress input is the same as the strain output resulting from the combined stress input.(84:82) The Boltzmann super position principle can be expressed with the following equation.

$$\varepsilon[\sigma_1(t) + \sigma_2(t - t_1)] = \varepsilon[\sigma_1(t)] + \varepsilon[\sigma_2(t - t_1)] \tag{2}$$

Viscoelastic Models

The mechanical response of viscoelastic materials has been modeled in terms of the elastic and viscous components by using traditional spring and dashpot methods.

Springs are typically used to represent ideal elastic behavior. When a load is applied to a spring it deforms a certain amount and when the load is removed the spring

returns to its original configuration, similar to a perfectly elastic bar. Hooke's law states that when a load or stress is applied to the spring there will be a resulting strain as shown in the following equation

$$\sigma_s = E\varepsilon_s \quad \textbf{(3)}$$

where E is the young's modulus. (25:4)

Dashpots are used to model ideal viscous behavior. The dashpot is a piston moving inside a frictionless cylinder. The more force that is applied to the piston the faster it will move. This is similar to viscous material and it is not the deformation that is important in this example rather it is the time rate of change that varies according to the force. Applying Newton's law to the dashpot we arrive at the equation

$$\sigma = \eta \frac{\delta\varepsilon}{\delta t} \quad \textbf{(4)}$$

where η is the viscosity and $\frac{\delta\varepsilon}{\delta t}$ is the strain rate and will be referred to further by $\dot{\varepsilon}$.

There are many different models to represent the behavior but three of the most common are the Maxwell model, the Kelvin-Voigt model, and the Three-element Standard Solid model.

Maxwell model

The Maxwell model consists of a spring in series with a dashpot. A representation of a Maxwell model is shown in Figure 6.

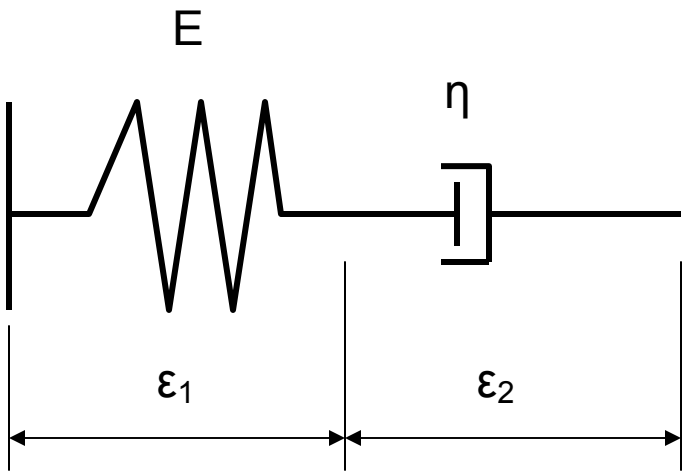

Figure 6: Maxwell model combining a spring and dashpot in series

Because the spring and dashpot are in series the total stress is equal throughout.

$$\sigma_T = \sigma_s = \sigma_d \tag{5}$$

The strain and the strain rate can be directly added to give the totals.

$$\varepsilon_T = \varepsilon_s + \varepsilon_d \tag{6}$$

$$\dot{\varepsilon}_T = \dot{\varepsilon}_s + \dot{\varepsilon}_d \tag{7}$$

During creep the stress remains constant. Applying Hooke's Law shown in equation 3 and Newton's Law in equation 4 along with the Equation for the total strain rate we can determine the strain rate under creep by the following equation

$$\dot{\varepsilon} = \frac{\dot{\sigma}}{E} + \frac{\sigma}{\eta} \tag{8}$$

Because the stress remains constant during creep testing we can say that $\dot{\sigma} = 0$. If we integrate this with respect to time and set the initial condition $\sigma = \sigma_0$ at $t = t_0$ the creep strain response can now be predicted by:

$$\varepsilon(t) = \frac{\sigma_0}{E} + \frac{\sigma_0}{\eta} t \tag{9}$$

This leaves $\frac{\sigma_0}{E}$ as a constant of integration based on the initial conditions. Just from looking at this equation you can see that the creep response predicted by the Maxwell model is linear as shown in Figure 7. This is not a realistic representation of creep in viscoelastic polymers.

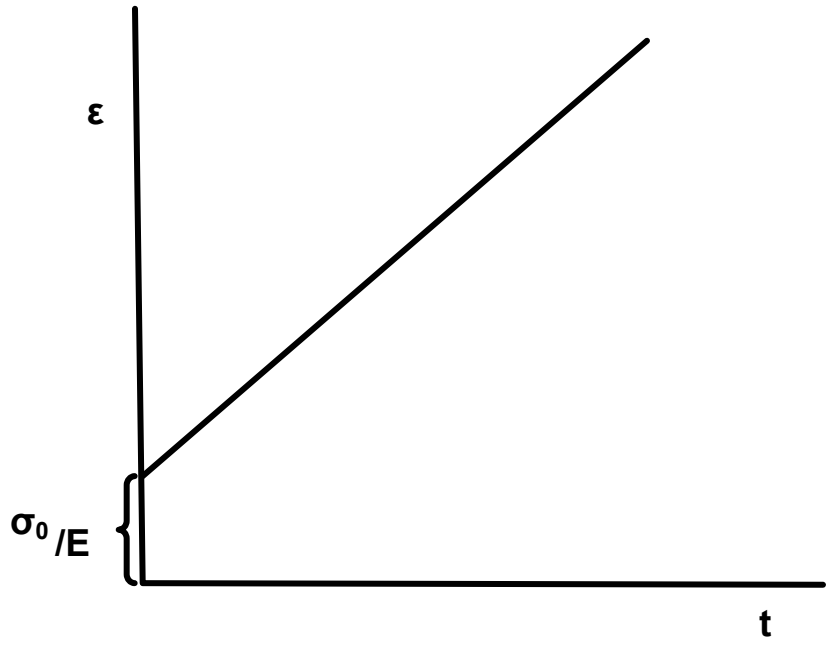

Figure 7: Maxwell model showing linear representation of creep. This model does not accurately predict viscoelastic behavior during creep

During stress relaxation experiments the material is loaded instantaneously to some strain ε_0 and studies the stress σ over time required to maintain the steady strain. Applying these initial conditions to Equation (9) we arrive at this equation

$$0 = \frac{\dot{\sigma}}{E} + \frac{\sigma}{\eta} \quad \textbf{(10)}$$

This equation is then simplified by multiplying both sides of the equation by the viscosity constant η and an integration factor $e^{\frac{E_t}{\eta}}$ is used. Integrating this resultant equation with respect to time leaves

$$\sigma(t) = -\frac{\sigma_0 E}{\eta} t + \sigma_0 \quad \textbf{(11)}$$

In this case σ_0 is the constant of integration. This equation gives the stress with respect to time during relaxation according to the Maxwell model. A graph of the relaxation stress vs. time is shown in Figure 8. (14:395-398; 26:141-143; 23:53-55)

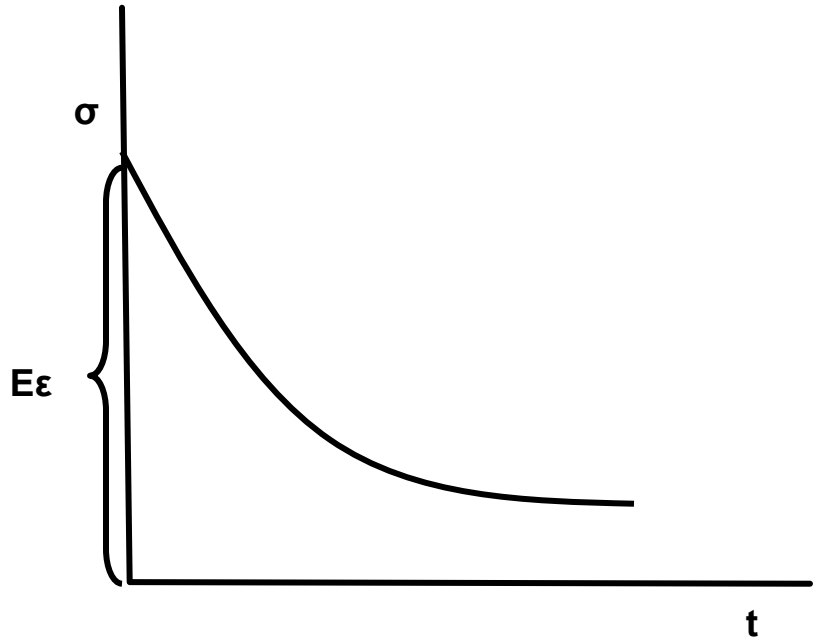

Figure 8: Maxwell model predicting the stress behavior as a function of time during relaxation.

Kelvin-Voigt Model

Another method for modeling viscoelastic materials is the Kelvin-Voigt model. It is similar to the Maxwell model in that it employs springs and dashpots. The difference between the two methods is that the Kelvin-Voigt model applies the spring and dashpot in parallel rather than in series like the Maxwell model. A representation of the Kelvin-Voigt model is shown in Figure 9.

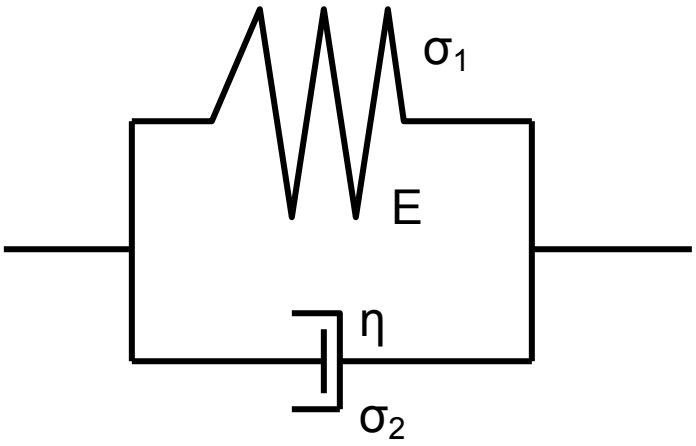

Figure 9: Representation of Kelvin-Voigt model a spring and Dashpot in parallel

The parallel configuration of the dashpot and spring in the Kelvin-Voigt model result in the stress, strain and strain rate equations are as follows

$$\sigma_T = \sigma_s + \sigma_d \quad \textbf{(12)}$$

$$\varepsilon_T = \varepsilon_s = \varepsilon_d \quad \textbf{(13)}$$

$$\dot{\varepsilon}_T = \dot{\varepsilon}_s = \dot{\varepsilon}_d \quad \textbf{(14)}$$

Now by applying Hooke's and Newton's law it can be written as

$$\sigma_T = E\varepsilon + \eta\dot{\varepsilon} \quad \textbf{(15)}$$

Dividing both sides of the equation by η and integrating with the integration factor of $e^{\frac{E_t}{\eta}}$ results in a solution for the prediction of strain during creep that is represented by

$$\varepsilon(t) = \frac{\sigma_0}{E}\left(1 - e^{\frac{-Et}{\eta}}\right) \quad \textbf{(16)}$$

The Kelvin-Voigt model accurately predicts the strain response during creep as shown in Figure 10. The strain increases at a decreasing rate and asymptotically approaching the value of $\frac{\sigma_0}{E}$ as t goes to infinity. The Kelvin-Voigt model response is that the load is first carried entirely by the viscous element and it elongates resulting in the steep strain curve at the beginning. As it elongates it transfers a greater portion of the load to the elastic element until the entire load is carried by the elastic element. This explains why the curve levels off as time increases. This behavior is called delayed elasticity. (23:55-56)

The Kelvin-Voigt model does not accurately predict relaxation. During relaxation the material is subjected to a constant strain $\dot{\varepsilon} = 0$, and equation 15 reduces to

$$\sigma_T = E\varepsilon \quad \textbf{(17)}$$

This shows that for a constant strain input there is a constant stress. This illustrates why the Kelvin-Voigt is not capable of modeling relaxation behavior. (14:398-399, 25:4-7, 26:147)

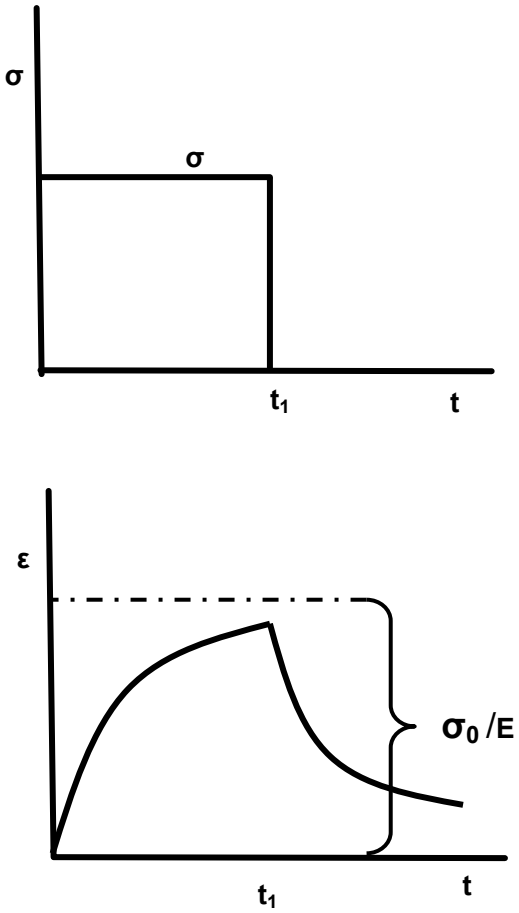

Figure 10: Schematic of the strain response for steady stress creep and recovery at zero stress as predicted by the Kelvin-Voigt model

Three-element Standard Linear Solid

The Maxwell model and the Kelvin-Voigt have limitations to predicting viscoelastic behavior. The Maxwell model is able to predict relaxation but does not do an accurate job of predicting creep. The Kelvin-Voigt model more accurately predicts the creep phase but is incapable of modeling the relaxation phase. To address the limitations of these other models, more complex models have been used to better approximate the behavior. What is commonly referred to as the Three-element standard solid, or standard

solid, is a combination of a Kelvin-Voigt model element in series with a spring. This model is able to more accurately predict behavior both in the creep phase and in the relaxation phase. A schematic of the three-element standard solid is shown in Figure 11.

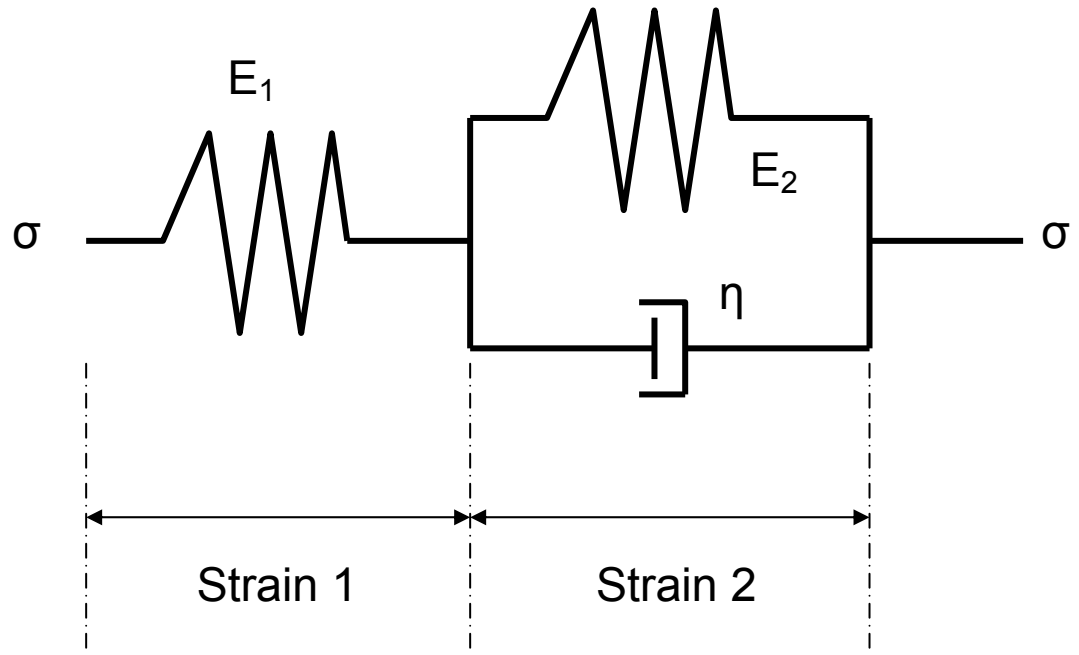

Figure 11: Three-element Standard Linear Solid Model

Using this model you must treat the two elements separately to determine the governing equations. The first element is the spring and the resulting equation is

$$\sigma_1 = E_1 \varepsilon_1 \quad \textbf{(18)}$$

The second element in the model is the spring and dashpot element which is a Kelvin-Voigt model. The resulting governing equations for this element are

$$\sigma_{E_2} = E_2 \varepsilon_2 \quad \textbf{(19)}$$

$$\sigma_\eta = \eta \dot{\varepsilon} \quad \textbf{(20)}$$

$$\sigma_2 = \sigma_{E_2} + \sigma_\eta \quad \textbf{(21)}$$

And the overall governing equations for this model are

$$\sigma_T = \sigma_1 = \sigma_2 \quad \textbf{(22)}$$

$$\varepsilon_T = \varepsilon_1 + \varepsilon_2 \quad \textbf{(23)}$$

$$\dot{\varepsilon}_T = \dot{\varepsilon}_1 + \dot{\varepsilon}_2 \quad \textbf{(24)}$$

Combining all of these governing equations and relating them to the total strain rate Equation (24), the equation for the strain response due to creep is

$$\dot{\varepsilon} + \frac{E_2}{\eta_2}\varepsilon = \frac{\dot{\sigma}}{E_1} + (1 + \frac{E_2}{E_1})\frac{\sigma}{\eta_2} \quad \textbf{(25)}$$

Taking into consideration that during creep the stress remains constant, $\dot{\sigma}$=0, and using the integration factor of $e^{\frac{E_2}{\eta_2}}$ and the initial condition that at time t_0, $\varepsilon = \frac{\sigma_0}{E_1}$ equation 25 becomes

$$\varepsilon(t) = \sigma_0\left(\frac{E_1 + E_2}{E_1 E_2}\right) - \frac{\sigma_0}{E_2}e^{-\frac{E_2}{\eta}t} \quad \textbf{(26)}$$

This is the three-element standard solid result for strain response due to creep.

The three-element standard model also holds up during the relaxation phase. During relaxation the stress varies and the strain is held constant, $\dot{\varepsilon}$=0. Applying this constraint to equation (25) the resulting equation is

$$\frac{E_2}{\eta}\varepsilon = \frac{\dot{\sigma}}{E_1} + \left(1 + \frac{E_2}{E_1}\right)\frac{\sigma}{\eta} \quad \textbf{(27)}$$

Applying an integration factor and integrating with respect to time and solving for the stress equation 27 breaks down to

$$\sigma(t) = \left(\frac{E_1 E_2}{E_1 + E_2}\right)\varepsilon + \left[\sigma_0 - \left(\frac{E_1 E_2}{E_1 + E_2}\right)\varepsilon\right]e^{-\left(\frac{E_1 + E_2}{\eta}\right)t} \quad \textbf{(28)}$$

Where the Kelvin-Voigt model reduced down to Hooke's Law and was incapable of predicting behavior during relaxation, the three-element standard model shows a much more accurate behavior during this phase.

And while the three-element standard solid does a better job of modeling all of the phases of a viscoelastic material, it is not the most accurate model. There are many more complex models that are used to more accurately model this type of behavior; however they are mainly deviations of these three models. The more complex models add more springs and dashpots in series and parallel to better model the behavior. (84:400-403)

Modeling is an important process that is used to accurately predict the behavior of composites over their useful lifespan. Depending on what material you are using experiments can be expensive or simply not possible to conduct. An accurate model based on known data can be used to predict the behavior of the material in different applications and save money in the long term.

Applications in Aerospace Structures

When determining materials for aerospace applications three main concerns drive the equation. These concerns are safety, cost, and weight. The ultimate goal of any aircraft is to be lighter. This increases the overall performance of the aircraft in maneuverability and range. Composite materials are the best answer for lighter materials. However cost and safety have been the reasons for a relatively slow adoption of composite materials in aircraft construction. Composites were used in very limited aerospace applications as early as WWII. But it was not until the 1960s when new glass fibers and boron fibers

were introduced which had greater stiffness and strength characteristics that composite use in aerospace applications started to increase. (33:436)

Because composite technology was still new and the cost of manufacture was extremely high in the early stages of development, the military has been the leader in composite technology for aerospace applications. The military has the advantage of focusing on performance and does not have to worry about being profitable as compared to commercial airlines. The high-stiffness boron and graphite fibers embedded in epoxy resins that became available in the late 1960s, were used by the U.S. military on rudders, ailerons, and other movable parts that control the motion of aircraft. The first major military production use of composites was for the horizontal stabilizers on the Navy's F-14 Tomcat interceptor which had its first flight in 1970. By 1981, the British Aerospace-McDonnell Douglas AV-8B Harrier flew with over 25 percent of its structure made of composite materials. (34)

The military has continued to stay at the forefront of composite materials in aerospace applications. Due to its stealth requirement, the B-2 bomber is an almost all-composite structure. This was done to meet a very specific design need and is not fiscally reasonable to be recreated on a large scale yet, but the technology is becoming available. The designers of the F-22 originally planned to use composite materials for 50% or more of the overall aircraft. The final design of the plane was only able to incorporate composites into 24% of the airframe while metals still accounted for 64%.(12:188) As composites continue to develop increased temperature resistance, and strength, they will have even greater presence in advancing aerospace designs and this trend is already transferring to the commercial sector.

Carbon Fiber composites started being used heavily in commercial aircraft in the early 1980s. Boeing introduced carbon fiber skins and other secondary load components in their 757 and 767 airframes. (7:36). As advances in composite technology continued to grow composites began being used in primary structures. Increased strength and better temperature resiliency combined with more cost effective ways of producing carbon fiber composites allowed them to be used in primary structures starting in the late 1980s. Airbus used carbon composites in the A320 empennage components. The composite used was a carbon/epoxy laminate skin. (7:36)

Since the late 1980s composites have made a steady and rapid increase in commercial aerospace applications. Boeing made the largest push to use composites in primary structures with the design of the 777, which had its maiden flight in 1994. “The major area in which composites were used as a primary structure for the first time was in the tail assembly.” The front and main tail spars are made out of carbon-fiber reinforced composites and the skin panels are also composites. Only the rear auxiliary spar is made out of aluminum.(11:59) The extensive use of composites in the tail section alone reduces the weight of the aircraft by 1650 lbs and increases the available range by 78 mi.(11:42)

Airbus has continued the trend toward increase usage of composites in their latest airframe the A380. The A380 uses carbon fiber reinforced plastic (CFRP) composite materials in the wing carry through structure as well as in the skin, tail and wing sections. The carry through wing structure represents the most complex, and critical aerospace composite structure ever attempted in civil aircraft applications. (33:437) Boeing looks to recapture the lead on composite materials usage with its 787 model. The 787 will become the first commercial aircraft with composite wings and fuselage. Boeing has attempted to

meet the original F-22 goal of composites being used for 50 percent of the aircraft's structural weight. (36) It is clear to see the road ahead for aviation design is composite materials.

Previous Work

There have been many studies on the effects of prior aging on the physical properties of composites. Dr Kong conducted tests that showed that thermal aging of graphite/epoxy composites below the glass transition temperature had an effect on the material properties of the composites. The Ultimate Tensile Strength, the strain to break, and the toughness of the composite all decreased as a function of the aging time.(4) Dr. Kong's research suggested that the physical aging of the matrix epoxy be considered when determining the durability of a composite.

Follow on studies have been conducted on different polymers and carbon fiber reinforced polymers with similar results. In the case of the carbon fiber composites research was done to determine how much of the degradation was due to the matrix and how much was due to the fibers. A study conducted by Le Coustumer determined that degradation of the material properties of the carbon fiber reinforced composite was due to oxidation that occurs during the aging process. The aging process was further broken down in his study to determine where the degradation occurs. The study was conducted on a bismaleimide matrix reinforced with carbon fibers with a 60% fiber volume ratio. This material is similar to the IM7/BMI 5250-4 material that was used in our testing. Le Coustumer's results showed that when aged at 250º C for 2500 hours degradation first occurred on the matrix only. This attack on the matrix is responsible for a noted weight

loss early in the aging process. As the matrix degrades there is less protection for the fibers and they began to degrade. In Le Coustumer's case the matrix had degraded enough after 600 hours to allow the fibers to begin to oxidize and degrade. (2)

Further studies into aging of bismaleimide composites were conducted by Bronwyn Fox. The results of these tests agreed not just with the decrease in material properties but also with the effects of aging on the composites. Fox determined that the greatest amount of damage to the composites due to aging occurred in the first 4 days of aging when aged at 250ºC. This study linked the degradation of the matrix to a decrease in composite interlaminar toughness. (3)

The effect of aging on composites is not unknown. It has been proven that aging will adversely affect the material properties of the composite. However everyday new thermosets are being developed to achieve higher continuous operation temperatures while still maintaining its material properties. It is important to continue research to determine the effects of aging for each composite to determine uses for them in the aerospace industry.

Thesis Objective

The purpose of this thesis was to determine the effects of prior aging on IM7/BMI 5250-4 composites. The specimens were weighed before aging to see what affect aging had on the material composition of the composite. Tests were conducted to determine the effects of aging on the Ultimate Tensile Strength of the composite. Creep tests were conducted to assess the effects of prior aging on the creep response. From these creep tests we were able to determine the effects that prior aging had on the stiffness of the composite. Creep-

recovery tests were conducted to determine how prior aging affected the percentage of creep strain recovered. The results of this work did seem to agree with previous results of similar tests conducted on other bismaleimide composites.

III. Material and Specimen

This section will address basic Prepreg technology, different methods of producing specimens from prepreg material and how our actual material was produced and manufactured into a testable specimen.

Prepreg Technology

Prepreg is short for preimpregnated materials. A prepreg consists of a matrix with fiber reinforcement. They are processed either in a unidirectional fiber form or with multiple direction reinforcement fibers. Prepregs are made from a variety of different resins and different reinforcing fibers depending on the applications they are going to be used for. Prepregs are currently used in everything from sporting equipment, marine and shipping applications to high performance aerospace components. Typical fibers used in aerospace applications are carbon fibers due to their high strength and stiffness and their low weight ratio. Of the different resins used in prepregs bismaleimides are most commonly used in aerospace applications because they have a higher service temperature (up to 260°C) compared to other resins. And they maintain their handling and toughness properties at these higher temperatures. (27)

The prepreg material used in this experiment was IM7/BMI 5250-4 manufactured by Cytec Engineered Materials. The resin is a 176° to 204°C curing Bismaleimide resin capable of continuous operation between -60° to 204°C.

IM7/BMI 5250-4 is specifically formulated for us in primary aircraft structures (15:1). Current applications of the material range from engine nacelles to wing and stabilizer spars to fuselage stiffeners and other critical load-bearing components.

The specimens that were tested were $[0/90]_{4s}$ and $[\pm 45]_{4s.}$ The Air Force material lab receives rolls of the material in its prepreg form. The material is then cut into 12” by 12” squares with the desired fiber orientation as shown in Figure 12.

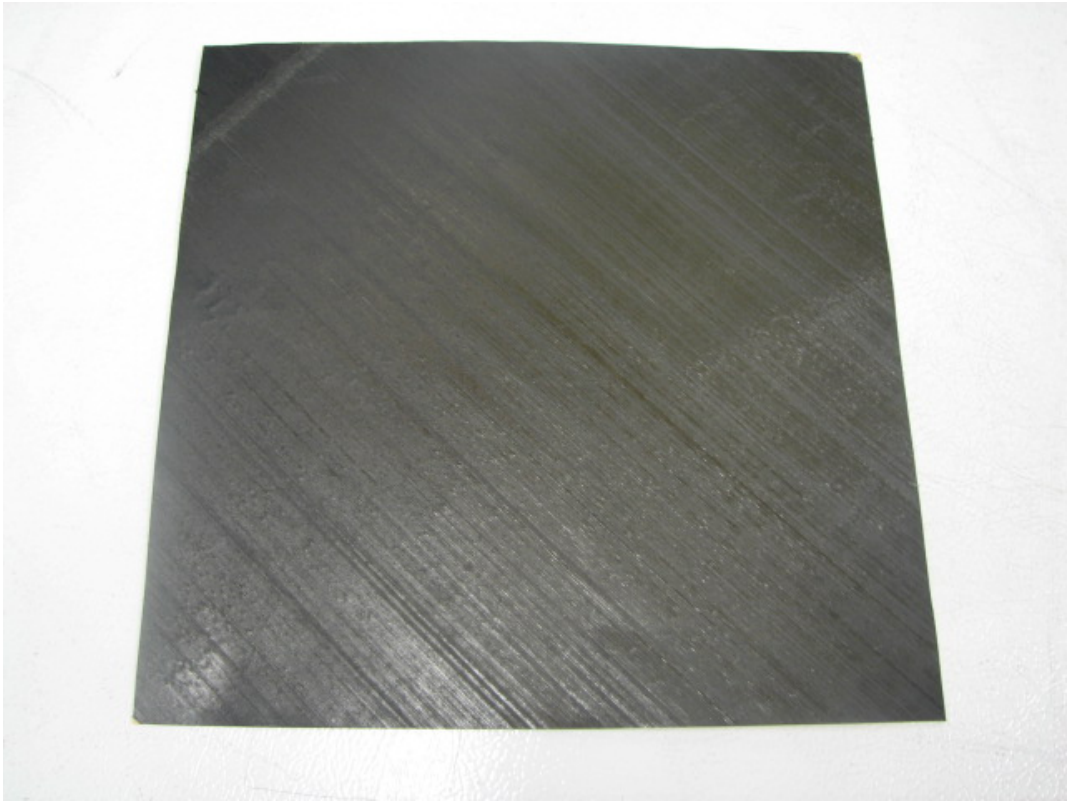

Figure 12: 12” X 12” Single Sheet of IM7/BMI 5250-4 Prepreg material cut at a 45˚ angle. Multiple sheets are stacked on top of each other, alternating fiber directions, to make up the composite.

The sheets of prepreg are then stacked on top of each other alternating the fiber orientation to give the desired specimen orientation. For this specimen there are a total of 16 sheets of prepreg. These sheets are then sandwiched between a porous Teflon material that gives the specimen a textured outer surface but which does not affect the material properties of the specimen. It also keeps the resin from sticking to the call plate. This layer of Teflon is called the release layer. The next step is to place a weighted call plate over the sheets and wrap the entire package in a non-porous Teflon material as shown in Figure 13.

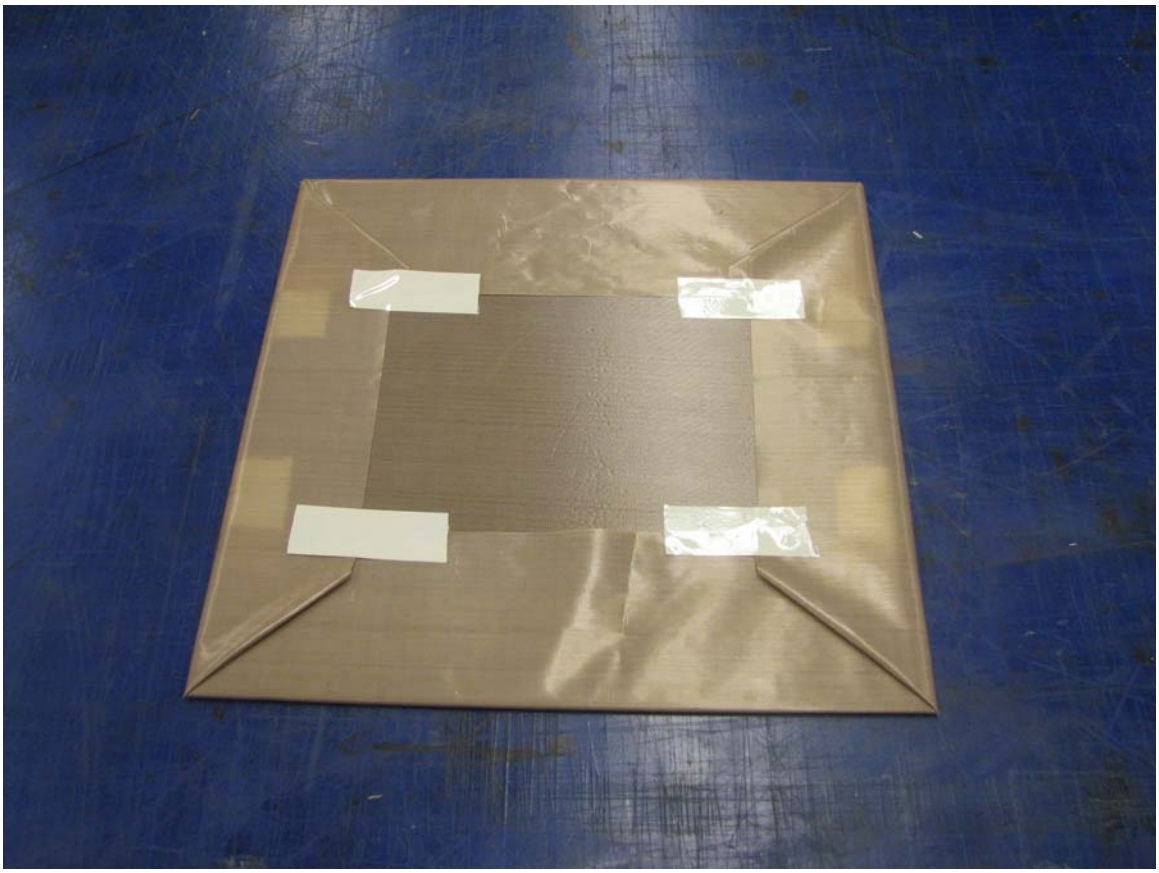

Figure 13: 12 X 12 Sheets of BMI IM7/5250-4 stacked together and sandwiched between porous Teflon with weighted call plate “gift wrapped” in non-porous Teflon for the autoclave

The package is placed inside a vacuum bag and inserted into an autoclave to cure. The vacuum ensures that no air pockets or other volatiles such as ethanol or acetone are present in the material before curing. These impurities cause weak points in the finished specimen. Figure 14 shows the vacuum process in the Autoclave.

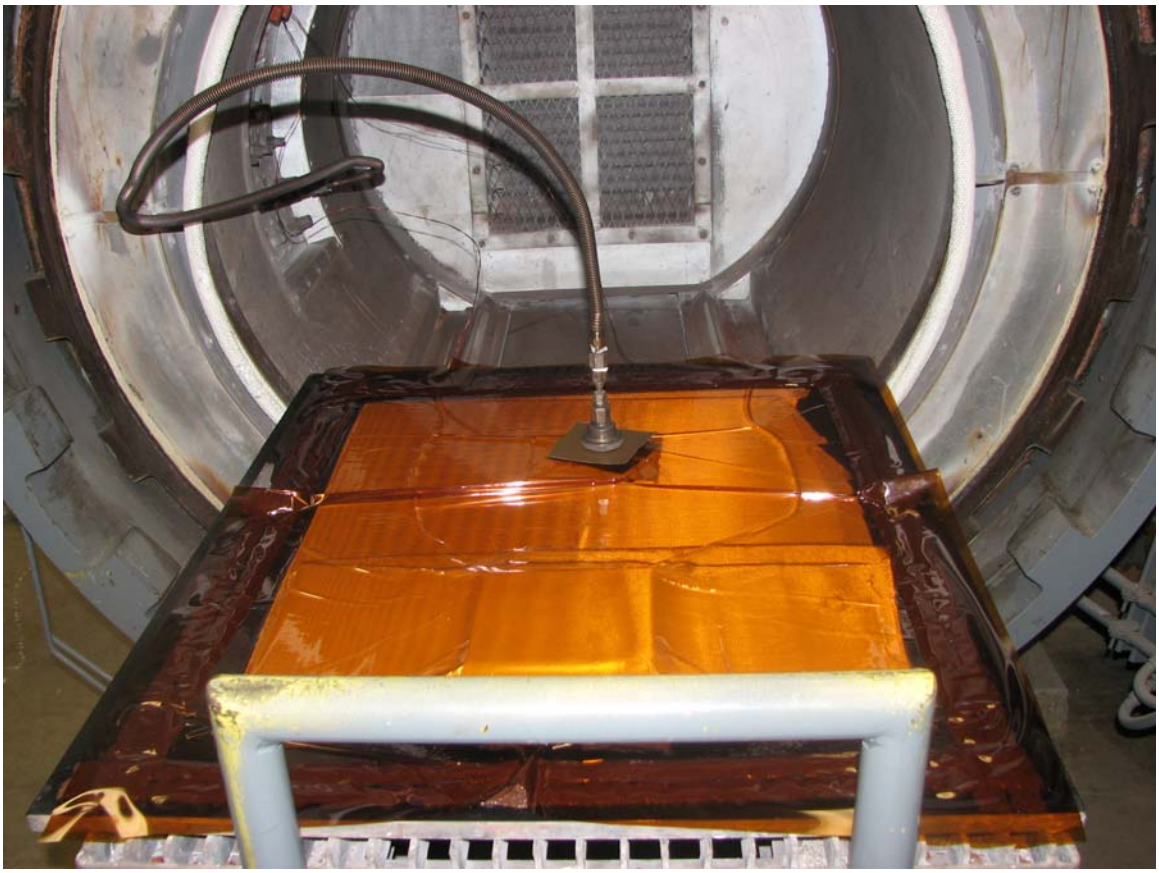

Figure 14: Gift wrapped sheets of BMI IM7/5250-4 placed inside a vacuum bag and being vacuum sealed before being put into the autoclave for curing

The material does its initial cure at 375˚F for 6 hours. As the material is heated, the resin will become a fluid. When the temperature reaches approximately 328˚F "the resin viscosity will reach a minimum and begin to rise as the increase in molecular size overcomes the temperature effect."(32:30) When the specimen reaches the hold temperature of 375˚F the resin forms a continuous cross-linked network. The material

will hold in this state for 6 hours to cure before it is brought back to room temperature. The material is then put through a post-cure for 6 hours at 440˚F to further strengthen the material panels.

The final step of the procedure is taking a C Scan of the finished panel to ensure that there are no impurities or weak points. The C Scan is the only way to detect any flaws in the material after it has been cured.

Test Specimens

The test specimens were machined at the Wright-Patterson Air Force Base machine shop according to the specifications in Figure 15 using a diamond tip blade. The diamond tip was used to give the cleanest edge when cutting through the fibers.

The specimens were cut into dog-bone shapes to provide wider ends for the vises to grip during the experiments as well as to define a narrower gage section to place maximum stress in the section where failure would first occur.

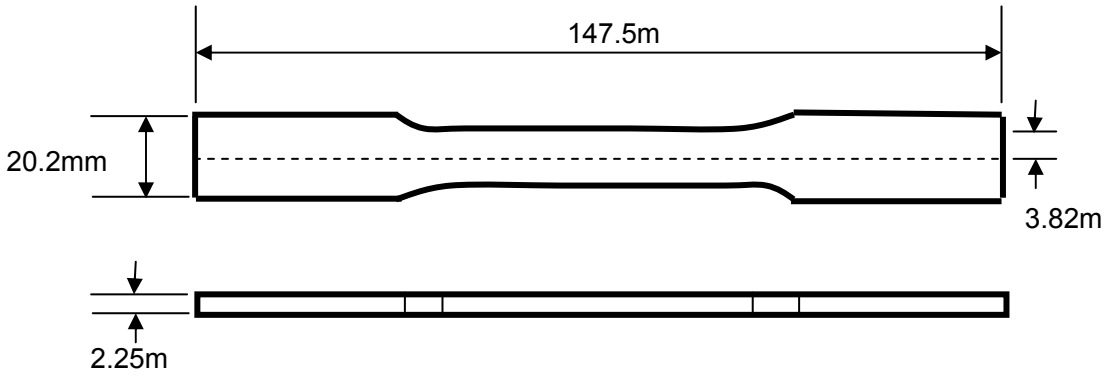

Figure 15: Final dimensions of the IM7/BMI 5250-4 test specimens that were machined with a diamond tip blade at the Wright Patterson Air Force Base machine shop

Aging

After the specimens were machined into the dog-bone shapes some of the specimens were taken back to the materials lab to be aged. The specimens were aged in air for 10 to 1000 hours. Other specimens were left unaged to act as a control group for direct comparison. The aging process consisted of placing the material in a vacuum oven for 48 hours. This step removed any final traces of moisture from the specimens. The specimens were then placed in a 375˚F oven for the desired time of aging. After the desired time has been reached the specimens were removed from the oven and stored in a dry-air-purged desiccator to keep moisture in the air from contaminating the specimens.

Test Preparation

Prior to testing, the ends of the specimens were tabbed with glass/epoxy material to prevent any damage to the specimens by the grips coming into direct contact with the specimen. The tabs were attached using M-Bond 200 adhesive. The final step to prepare the test specimen was to dimple the side of the specimen for the extensometer. A small dimpling tool was used to put 2 dimples 0.5” apart on the side of the specimen. These dimples provided contact points for the extensometer to attach to, and the dimples were small enough not to affect the strength or integrity of the specimen. A tabbed specimen is shown in Figure 16.

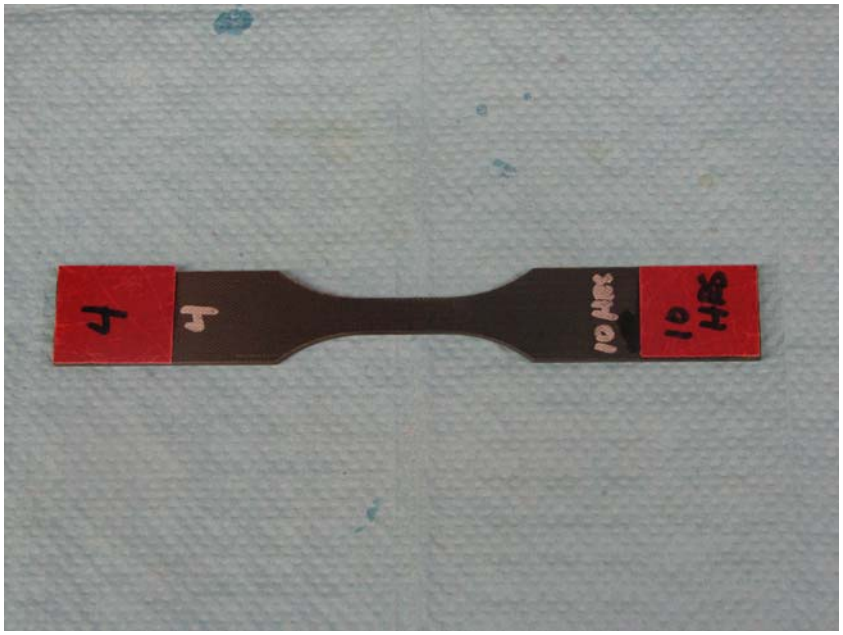

Figure 16: Dog-bone shaped IM7/BMI 5250-4 test specimen clearly illustrating the narrow gage section and shown with glass/epoxy tabs on the ends

IV. Experimental Setup and Testing Procedures

This section presents a detailed description of the experimental setup and specific test procedures used during this research.

Experimental Setup

The equipment used in the testing of these specimens consists of four separate components: the hydraulic machine with cooling system, extensometer, computer software, and the furnaces to heat the specimen. Each of these components is essential to the successful execution of the experiment and the accurate extraction of data.

The Mechanical Testing Machine

The servo-hydraulic machine used in the testing of all of the specimens was an 810 Material Test System (MTS) servo hydraulic machine. The machine had a maximum load capacity of 22 kips. The 22 kips machine was chosen to ensure that there was sufficient load capability for the specimens. After the experiments were conducted it was found that the largest load encountered was 14500 N or approximately 3.3 kips, well below the limits of the MTS machine.

Another integral part of the MTS machine is the hydraulic wedge grips. These hold the specimen in place during the experiment. The 810 MTS is equipped with Series 647.02B Hydraulic Wedge Grips.

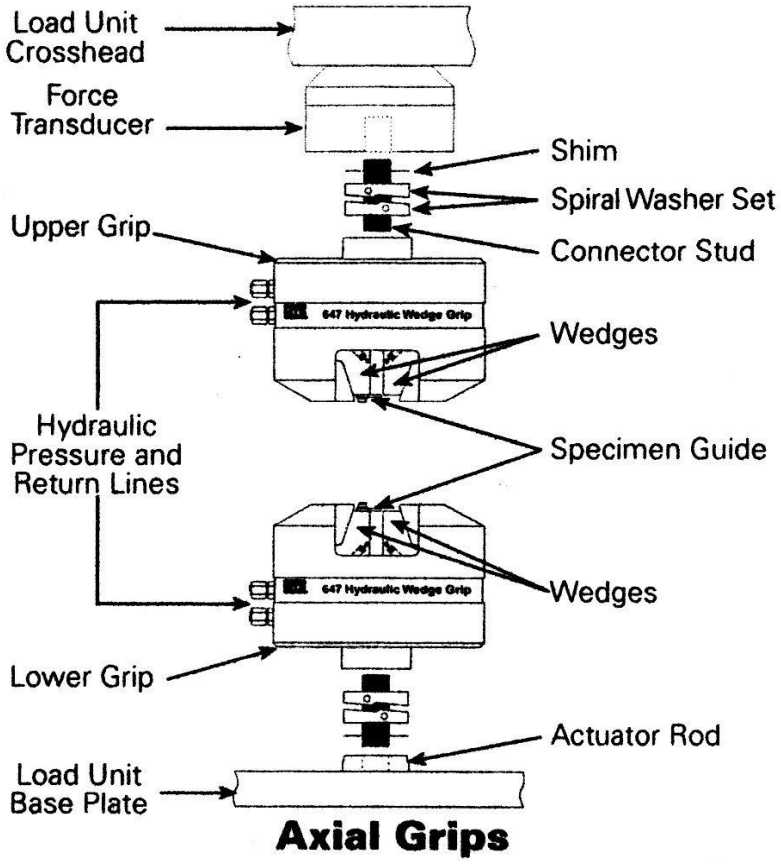

Figure 17: Schematic of 647.02B Hydraulic Wedge Grips

The maximum pressure we used for these grips was 21MPa (3,000 psi) (29) to avoid damaging the specimens from over gripping. The grips were fitted with flat wedges for testing our specimens; other types of grips can be fitted for different shaped specimens. The flat faces of the grips are coated with a Surfalloy which incorporates a grit onto the wedge surface, and provides better grip on the specimen.

The acceptable temperature range of the wedges is between -18˚ and 66˚C. Our specimens were tested at 191˚C. To avoid damage to the wedges they are fitted with a water cooling kit which includes inlets and outlets for water to cool the grips during the

high testing temperatures. (29) The grips were connected to a NESLAB thermo chiller to circulate and chill the water to stay between 9˚ and 24˚C, thus keeping the grips within their operating temperature range during high temperature tests. An anti-rotation device was also fitted onto the machine actuator to ensure purely tensile loading. Figure 18 shows the servo hydraulic system, the furnace, the cooling lines, and the extensometer assembly attached.

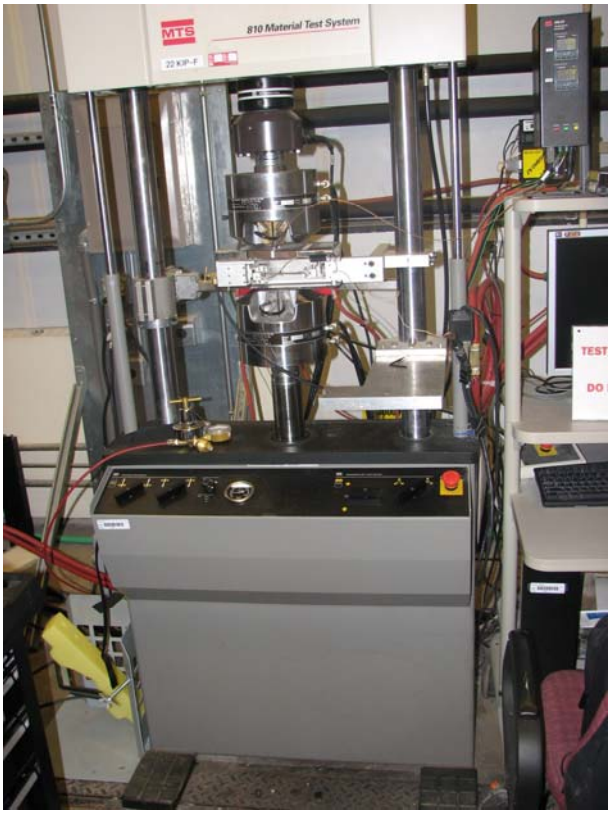

Figure 18: MTS Servo Hydraulic Machine with the extensometer heat shield installed and cooling lines running to the grips

Extensometer

An MTS Model 632.53E-14 uniaxial high-temperature low-contact force extensometer was used to obtain strain measurements during the testing. This model has an air-cooling option; however it was not necessary to use it because the maximum

operating temperature without cooling is 650˚C, much higher than the 191˚C that the testing was being conducted at. The gage length of the extensometer is 0.5 in and the maximum measurable strain range is -10 to +20 %.(30) The extensometer uses 3.50 mm diameter ceramic extension rods. These rods have a conical tip that allows the extensometer ceramic rods to fit into the dimpled specimen. The specimen is dimpled using an MTS punch fixture tool and the dimples are 0.5 in apart to coincide with the extensometer gage length. The extensometer is affixed to a support arm that is positioned behind a heat shield. This helps protect the extensometer from the heat of the furnaces during high temperature testing. Figure 19 (a) shows a detailed picture of the extensometer, and Figure 19 (b) shows the extensometer mounted behind the heat shield and the extension rods extended through the furnace to the test specimen.

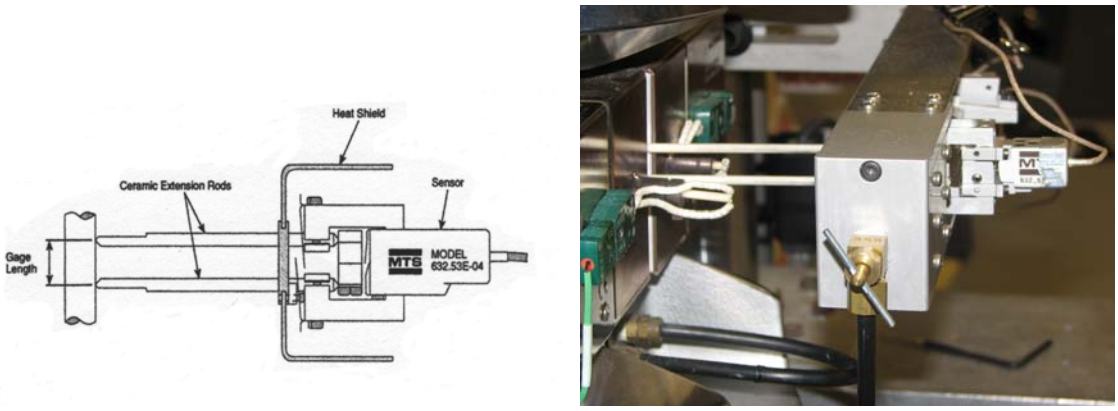

(a) **(b)**

Figure 19: Model 632.53 high temperature low-contact force extensometer (a) detailed illustration of the extension rods and the gage length (b) the extensometer connected to the specimen and installed behind the heat shield

Computer Software

The MTS Teststar II digital controller and MTS model 793 system software was used to run the test and acquire data. A configuration file was created for the specific type of

material being tested and the type of test being conducted. This configuration file contained all of the tuning parameters for each specimen and saved them for follow on tests. The MTS Multi-Purpose Testware (MPT) was then used to create procedures for each test. The procedures controlled the entire process from the heating of the furnaces to applying and holding the desired load all the way to completion of the test. The procedure also specified the data that was going to be collected and how it would be saved. An example of a typical procedure is shown in Figure 20.

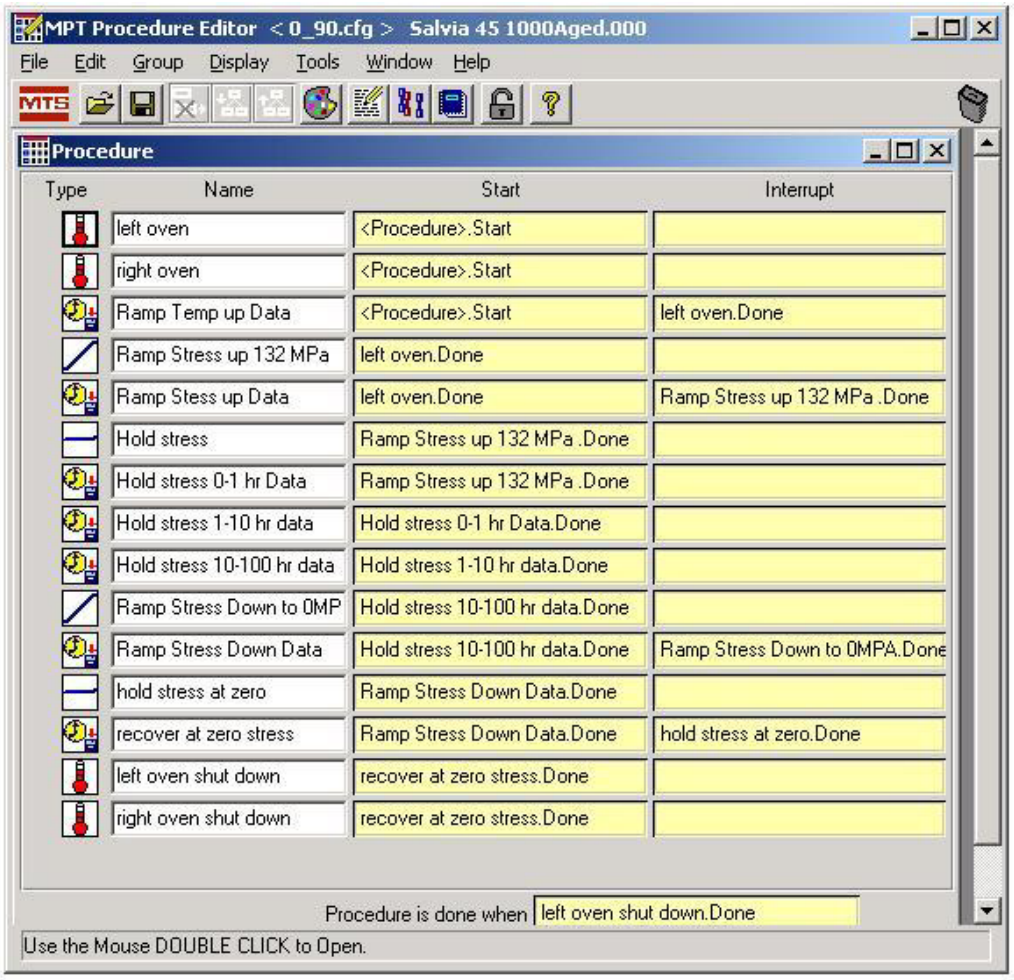

Figure 20: An example of a creep test procedure written in the procedure editor of the MTS model 793 system software displaying all of the commands for a complete test

Furnace

An MTS High Temperature Furnace was used to sustain the 191˚C that was required for the testing. The Furnace used was the MTS Model 653.02 which has 2 heating zones and an operating temperature range of 100-1400˚C. (31) The furnace utilizes a center-split design which provides easy specimen access. The furnace closes together on either side of the test specimen during testing. The heating elements are silicon carbide and provide rapid heating, and low heat loss. The temperature control for each half of the furnace is controlled separately using the MTS Test Software through the Model 409.83 temperature controller. There is a separate temperature controller for each side of the furnace. Each side of the furnace is equipped with a thermocouple which works in conjunction with the software and the controllers to keep the temperature constant during testing. Both sides of the furnace have insulation material made of polycrystalline alumina fiber. The insulation must be filed away to provide room for the specimen and the extensometer. The rest of the insulation must remain intact to help maintain a constant temperature. Because the furnace halves operate independently there may be a difference in the required temperature setting to achieve the desired temperature. In this case the left furnace was set to 186˚C and the right furnace was set to 178˚C to achieve the desired specimen temperature of 191˚C. This temperature difference between the furnace halves can be attributed to element wear. Figure 21 shows the furnace and the insulation that has been filed to accommodate the specimen.

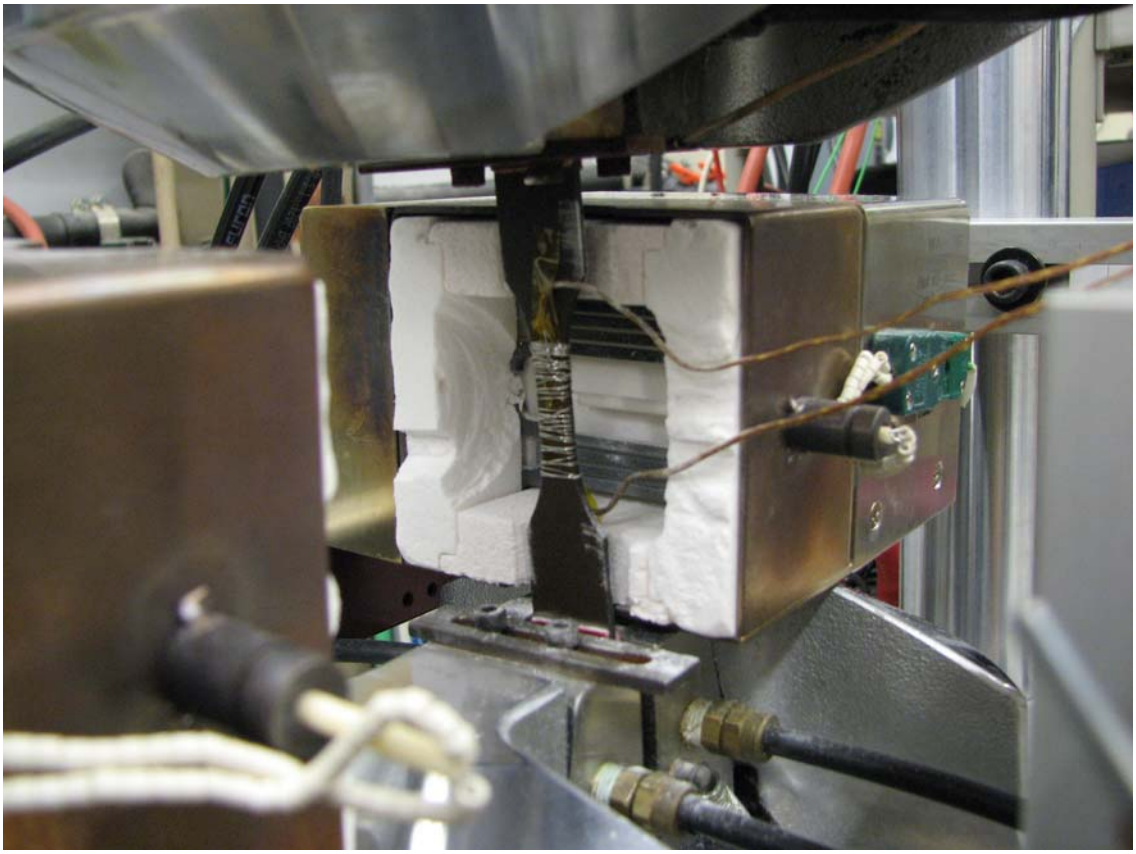

Figure 21: The right side of the MTS Model 653.02 Furnace with a test specimen placed in the grips and thermocouples connected for temperature calibration. Note the cooling lines attached to the front of the grips

Experimental Procedures

Prior to conducting any tests there were a number of steps that had to be completed to ensure accurate and safe results. The first step was to warm up the hydraulics by using the function generator to cycle the system at a low frequency for at least 30 minutes. The next step was to ensure that the chiller was turned on to ensure the circulating water was chilled enough to regulate the temperature during testing. While this warm up was being done the specimen gage section width and thickness were measured using a micrometer. These measurements were then used to calculate the load levels required to achieve the desired stress level for the test. These calculated load levels were then entered into the

procedure editor and saved to run the test. The next step was to dimple the sides of the specimen to allow the extensometer to hold securely in place during testing. The dimpling was done with an MTS supplied dimpling punch. The dimples were placed 0.5 in apart in accordance with the gage length of the extensometer. The specimen was then tabbed using the M-Bond. The grip pressure was set to the desired level to hold the specimen without slipping during testing and the specimen was placed in the grips. The MTS machine was placed in manual control and the bottom grip was raised to the zero displacement point which was predetermined during the configuration phase. The specimen was then placed in the top grips lining up vertically with the grip guides on the back of the grips. The manual control was then switched to force control and the load was zeroed out. The specimen was then gripped in the bottom grips. This order of things ensured that no load was being applied to the specimen prior to the start of the test.

The extensometer was then placed on the specimen ensuring that the extension rods were securely placed in the dimples and the strain gage read 0%. The interlocks must then be set and enabled to ensure that neither the specimen nor any other part of the testing system gets damaged during testing. The last step is to zero out the displacement and the strain readings before the test. The procedure that was saved prior was then run on the specimen. The machine was kept in the force control mode during heat up to allow the specimen to expand. Once the desired temperature was reached the specimen was put on dwell at that temperature for 30 minutes prior to applying a force. This dwell time allowed the specimen temperature to reach equilibrium.

Data Collection

The following data: Force (N), displacement (mm), strain (m/m), time (s) and Temperature of the left and the right furnace (˚C) were collected for every test that was run. Also the command signal was recorded depending on what type of test was being run. The tensile tests to failure were conducted in displacement control mode, and therefore the displacement command was recorded. The creep tests were conducted in the force control mode and it was the force command that was also recorded. The rate of data sampling varied during the different stages of the test to ensure the most accurate and usable data was collected. Table 3 shows the data sampling rates for the Creep Test Procedures.

Table 3: Data sampling rates for Creep test Procedures

Test Stage	Sampling Rate
Heat Up	2/min
Load Up	5/sec
Hold for 0-1 Hour	1/sec
Hold for 1-11 Hours	6/min
Hold for 11-100 Hours	2/min
Ramp Down	2.5/sec
Creep Recovery for 100 Hours	2/min

Temperature Calibration

The tests were all conducted at 191°C. Temperature calibration was completed prior to testing to determine the furnace settings to maintain 191°C on the specimen. Calibration was conducted using an Omega HH202A Temperature Scale with measurement ranges up to 1767°C depending on which type of thermocouple is used. The Omega Temperature Scale provides readings of two thermocouples simultaneously.

K-type thermocouples were used for this temperature calibration, which have an operating range from -50°C to 1372°C. The thermocouples were secured to both sides of the specimen using Kapton tape and wire to ensure that the tip of the thermocouples stayed in contact with the specimen.

Figure 22 shows a tabbed specimen with thermocouples attached. The ovens were set to increase temperature 2° every minute up to 75° and then hold for 30 minutes. The next step increased the temperature to 120° at 2° intervals with another 30 minute hold time. From this point the temperature was manually increased 1° every minute until both sides of the specimen reached 191°C. The temperature was increased at this slow pace to limit any overshoot of the desired temperature of 191° and also to determine any disparity between the two furnaces. Because the furnaces acted independently they had to be increased individually. The temperature calibration determined the left furnace should be set to 186° and the right furnace set to 178°. These settings resulted in both sides of the specimen being at 191°C. This disparity between the furnaces can be attributed to the furnace elements. The right side furnace elements had been replaced just prior to the temperature calibration. This can result in having to set the temperature lower to achieve more heat from the newer element, and this is what was noticed during the temperature calibration.

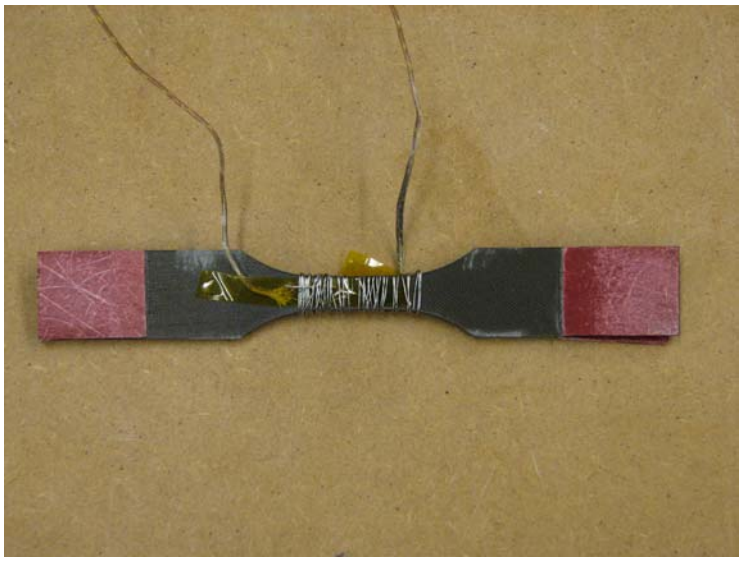

Figure 22: BMI IM7/5250-4 tabbed test specimen with K-type thermocouples attached with wire and Kapton tape to ensure constant contact with the specimen

Tuning

Proper tuning improves the performance of the test system by reducing the error and phase lag between the program command and the sensor feedback. This ensures that when a force command is given the correct force is applied smoothly with very little undershoot or overshoot and no oscillations. Because of the very different performance attributes of the two specimens, tuning had to be conducted for the [0/90] configuration and for the [±45] configuration. All of the creep tests were conducted in the force control mode so the tuning was also conducted in the force control mode. To tune in the force control mode a specimen had to be placed into the machine. Using the tuning software a cyclic load was applied to the specimen with the maximum load being 10% of the Ultimate Tensile Strength of the specimen and a frequency of 0.75HZ. For the [0/90] specimen the cyclic load ranged from 50N to 950N with a mean of 500N and amplitude of 450N. The [±45] specimen ranged from 50N to 300N with a mean of 175N and amplitude of 125N. The Oscilloscope was monitored to compare the force command with

the actual force being applied. Tuning in the force control mode allows for adjustment of five different settings to achieve an actual force being applied that most closely resembles the force command. The Proportional Gain (P Gain) is used to improve system response. A higher P Gain increases the speed of the system response. If the P Gain is too high the system can become unstable and if the P Gain is too low the system will be sluggish. Integral Gain (I Gain) increases system response during static or low-frequency operation. Higher I Gain settings improve system response time, however excessive I Gain can cause overshoot and oscillation. Derivative Gain (D Gain) introduces a derivative of the feedback signal and reduces ringing. It is only used with dynamic test programs. Feed Forward Gain (F Gain) introduces a derivative of the command signal. Forward Loop Filter (FL Filter) adjustments compensate for noise in the servo loop, which usually comes from sensor feedback. (Model793.00 System Software: 524-531) The tuning parameters for the [0/90] and the [±45] specimens are shown in Table 4 and Table 5.

Table 4: Tuning Parameters for [0/90]

Tuning Parameter	Value
P Gain	0.6
I Gain	0.11
D Gain	0.00
F Gain	0.00
FL Filter	2048.0 Hz

Table 5: Tuning Parameters for [±45]

Tuning Parameter	Value
P Gain	0.85
I Gain	0.11
D Gain	0.00
F Gain	0.00
FL Filter	2048.0 Hz

Monotonic Tensile Test

Monotonic tensile tests to failure were conducted on both the [±45] and the [0/90] unaged specimens. These tests were conducted to determine the Ultimate Tensile Strength (UTS) of each specimen. The tests were conducted at 191°C in the displacement mode. The results of these tests were used to determine the desired level of stress that would be used on all other subsequent creep tests.

Tensile tests to failure were also conducted on both orientations of specimens for each aged group to assess the effects of aging on the UTS of the composite.

Creep Test

Creep tests were conducted at 191˚C on unaged [±45] specimens to determine what percent of UTS should be used for all subsequent testing to give the most useful data. The tests were conducted in the force control mode. The load was applied at a rate of 2 MPa/sec to reach the desired percentage of UTS in the minimum amount of time to simulate instantaneous loading while minimizing overshoot.

The initial creep test was conducted at 80% UTS. The specimen did not fracture and achieved run out of 100 hours. Another Creep test was performed at 88% UTS on a [±45] unaged specimen. This specimen fractured in less than 60 seconds. A third test was conducted at 85% UTS and this specimen fractured after only 150 seconds. Based on these results it was decided that the 85% and 88% UTS creep tests would not provide enough data points to sufficiently compare the effects of aging on the creep response of the specimens. Therefore all subsequent creep tests were performed at 80% UTS. Figure

23 shows a graphical representation of the creep tests conducted on the unaged specimens to determine the percent of UTS that would be used to conduct all of the subsequent tests.

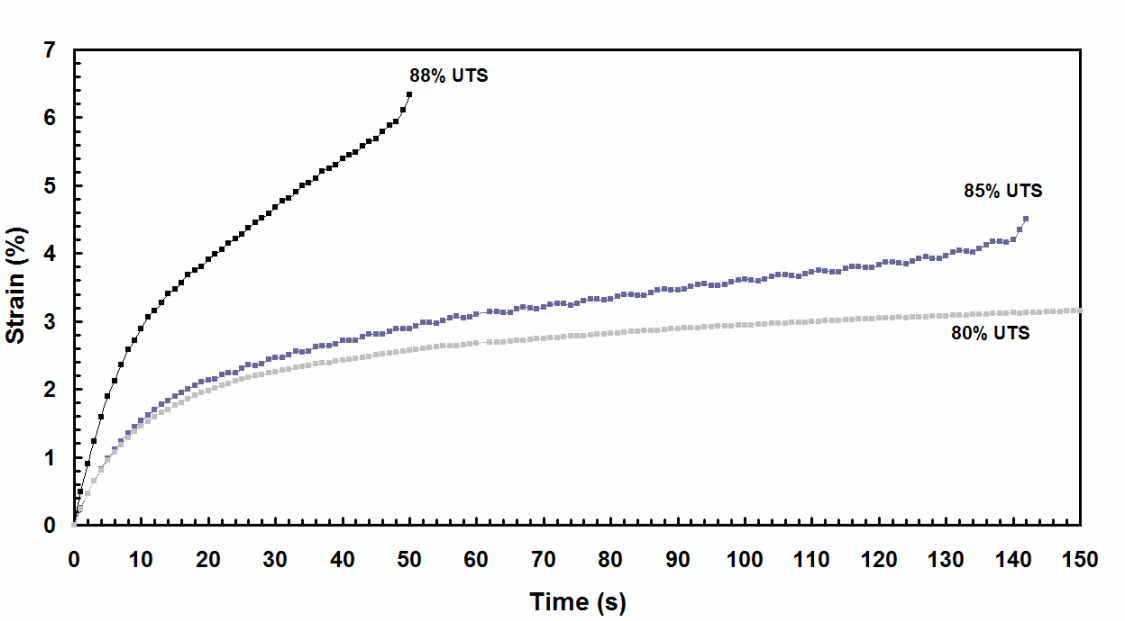

Figure 23: Percent of strain as a function of time for unaged [±45] IM7/BMI 5250-4 specimens subjected to creep tests at 80%, 85%, and 88% UTS

The same 80% UTS creep test was then performed on the [0/90] unaged specimen. The creep response for this specimen was negligible due to the fiber orientation dominating the entire specimen. The test was conducted for both the unaged and a specimen that was aged 1000 hours. Both of the creep responses were minimal for this fiber orientation.

Recovery at Zero Stress

Recovery tests were conducted on the unaged [±45] specimen and the 1000 hour aged [±45] specimen. Both of these specimens reached run out of 100 hours during the creep test at 80% UTS. The recovery tests consisted of returning the applied load back to

zero and holding the specimen at zero load for 60 hours. This test was performed to assess the effects of prior aging on how much of the overall creep strain would be recovered. Also this test was able to show if any permanent damage was sustained by the composites during the creep tests.

V. Results and Discussion

This chapter summarizes all of the results of the research completed. It first addresses the effect of aging on weight as well as on Ultimate Tensile Strength (UTS) and Young's modulus of the specimens with different fiber orientations.

Effects of Aging on Specimen Weight

The specimens were all aged at 191°C in air for periods of time ranging from 10 to 1000 h. Before the aging process the specimens were stored in a dry-air-purged dessicator to minimize moisture content before testing. Prior to aging eight control specimens (4 of each fiber orientation) were weighed using a micro balance scale with an accuracy of 0.0001 grams.

Prior to aging all the specimens were placed in a vacuum oven at 191°C for 48 hours in order to remove all of the moisture. Thus all of the specimens had a near equal low moisture content at the start of aging. This is important because the specimens came from different panels of the same material and could have been subjected to different environmental conditions prior to aging. The eight control samples were weighed again immediately following the vacuum oven stage.

The next step in the aging process was to place the specimens in a 191˚C oven for the desired period of aging time. The control specimens were weighed periodically throughout the aging process to determine how specimen weight changed with aging time. Only the control specimens were weighed during the aging process. Because the aging process was the same for all specimens, the weight measurements obtained for the

control specimens reflect the weight change with aging time for the entire specimen population. Weight of control specimens as a function of time is represented in Figure 24.

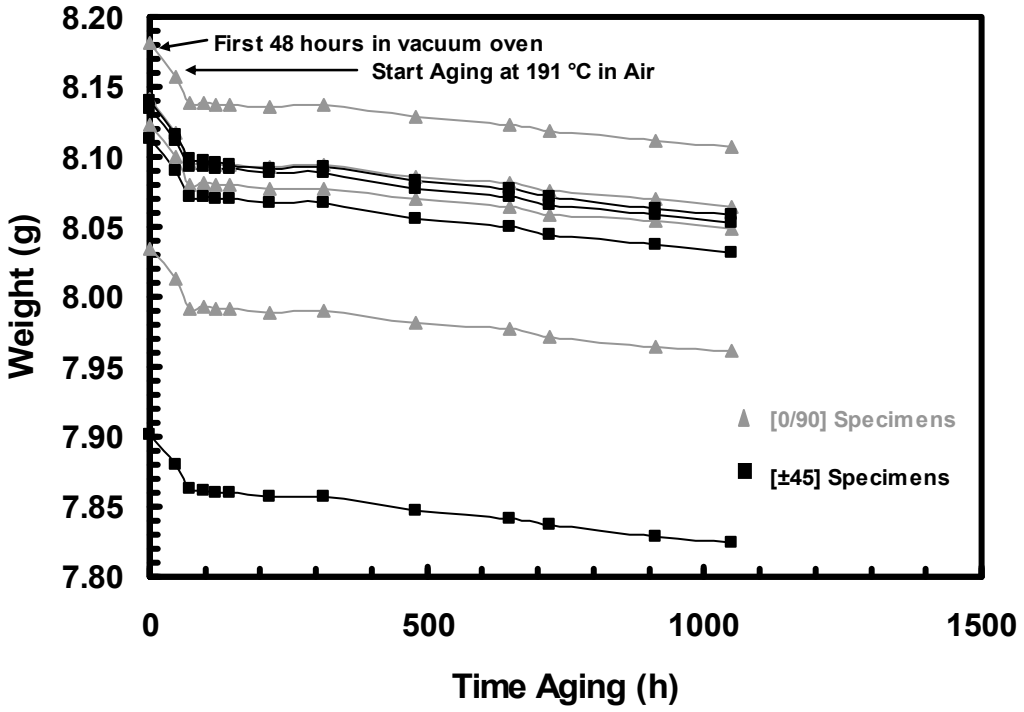

Figure 24: Weight loss in grams as a function of time aging in air at 191˚C for [±45] and [0/90] fiber orientations of IM7/BMI 5250-4

The first 48 h on the graph in Figure 24 depict the time that the specimens spent in the vacuum oven. This corresponds to the most significant weight loss. Nearly one third of the total overall weight loss occurred during this phase. After 48 h in the vacuum oven phase the specimens were placed inside the oven for aging treatment at 191˚C. The next significant and the most rapid weight loss occurred during the first 24 h. These Percentages can be seen in Figure 25 which depicts the percentage of weight loss as a function of time.

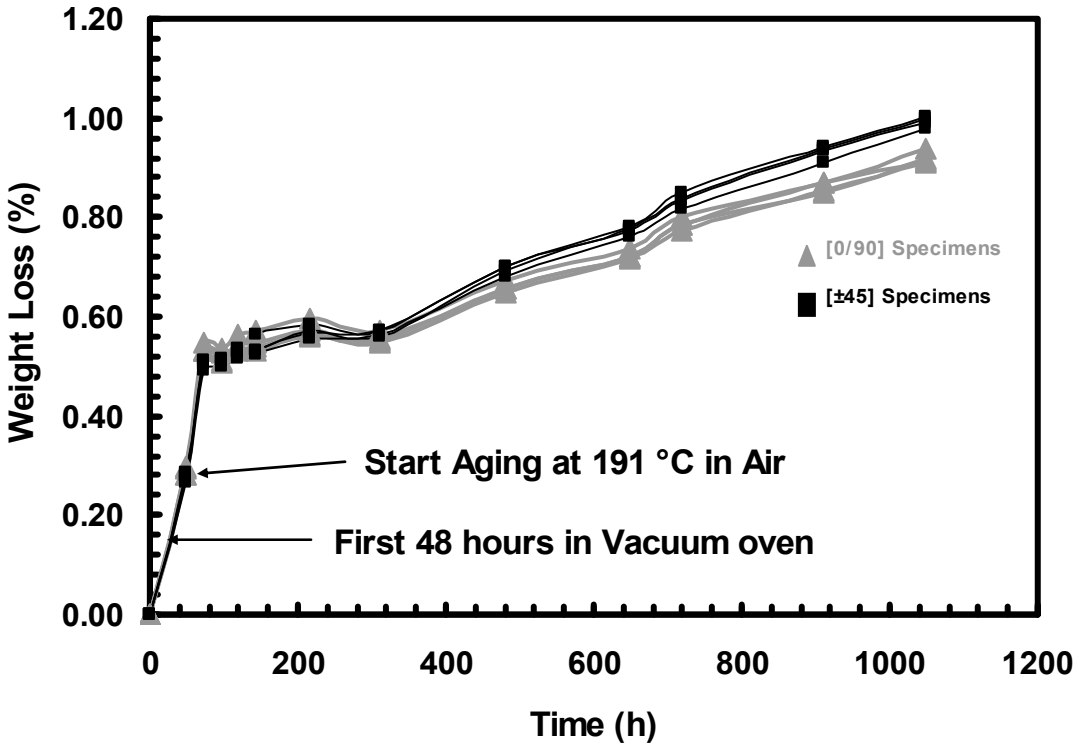

Figure 25: Percent weight loss as a function of time aging in air at 191˚C for [±45] and [0/90] fiber orientations of BMI IM7/ 5250-4

The specimens continued to lose weight over the next 1000 hours but at a much slower rate than the first 24 hours. The percentage of weight loss was similar for the eight control specimens as seen in Figure 25.

The weight loss of the specimens is attributed to the weight loss of the matrix. During the vacuum oven treatment and during the aging process the matrix loses moisture quickly. The amount of weight loss for the [±45] fiber orientation specimens was slightly higher than the [0/90] specimens. This is expected and is supported in a study performed by Dr. Schoeppner on PMR-15 composites. (35) He found that the oxidation layer and the damage to the free surfaces increased with time and demonstrated

that debonding of the fiber and matrix as well as matrix cracking provided added pathways for oxidation. (35) This explains the rapid weight loss early in the aging process. The [±45] specimens had more entryways for the environment to enter the specimens because of the orientation of the fibers. This is shown in Figure 26.

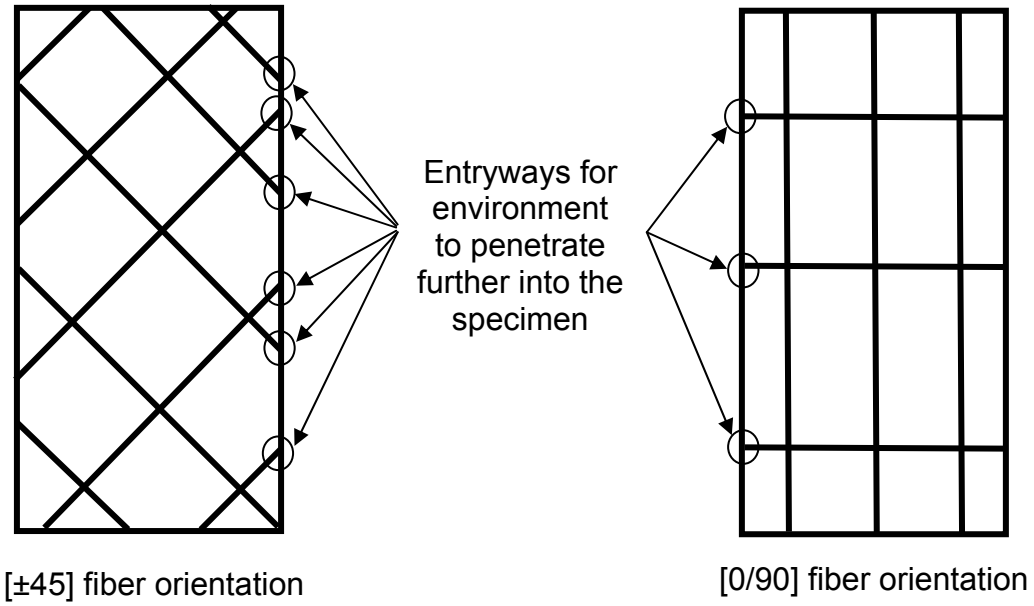

Figure 26: Schematic of [±45] and [0/90] specimens of BMI IM7/5250-4 showing the number of entryways where atmosphere can penetrate deeper into the specimen during the aging process

Breaks or cracks in the matrix allow for more rapid aging and weight loss. The points on the sides of the specimens where the fibers are exposed are breaks in the matrix and are entryways for the environment to penetrate deeper into the specimen and cause more rapid aging on the entire specimen. The [±45] specimens have more of these entryways

and would therefore be expected to age at a more rapid pace than the [0/90] specimens. This is supported by the results shown in Figure 25. The percent of weight loss due only to aging differed between the two fiber orientations. The [±45] fiber orientations lost 0.72% while the [0/90] fiber orientations only lost 0.64%.

The specimens were returned to the dry-air-purged dessicator after aging and remained in there until testing. This was done to ensure that moisture from the environment would not be absorbed by the specimens before testing.

Tensile Tests to Failure

Tensile tests to failure were first conducted at 191°C to determine tensile properties, such as Ultimate Tensile Strength (UTS), modulus, and failure strain. Tensile tests to failure were conducted on both the unaged and the aged specimens to assess the effect of prior aging on tensile properties and stress-strain behavior.

For the [±45] fiber orientation, the UTS was 165 MPa. Figure 27 shows the tensile stress-strain curve obtained for the [±45] specimen at 191°C.

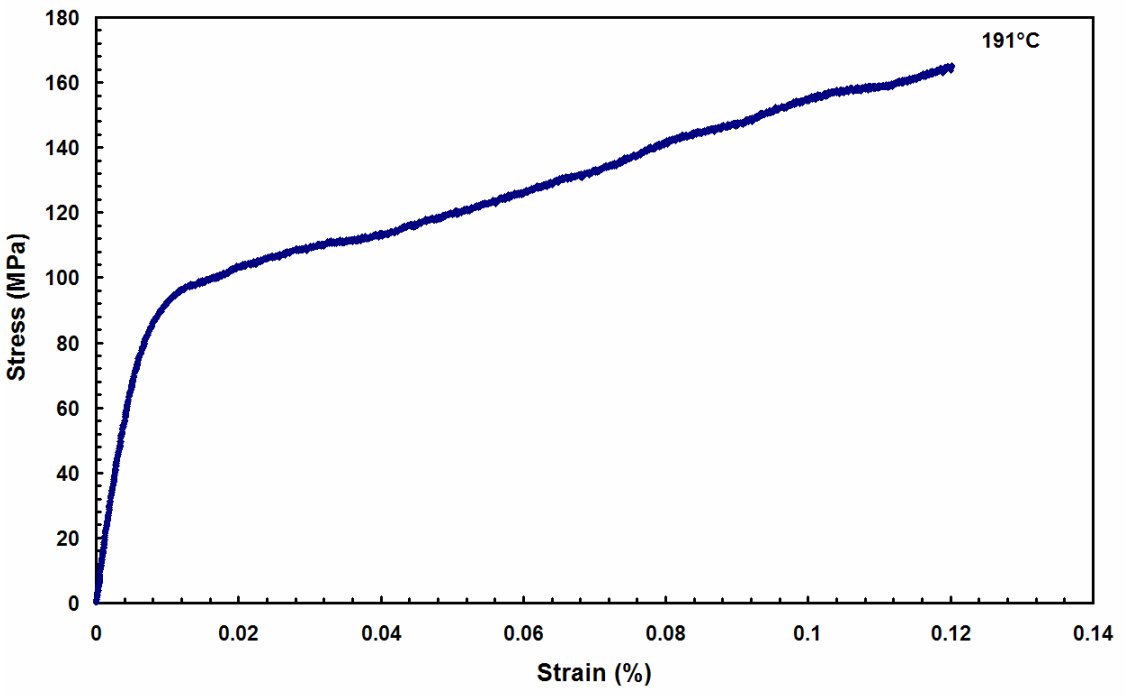

Figure 27: Tensile stress-strain curve for the unaged IM7/BMI 5250-4 specimen with [±45] fiber orientation at 191˚C

Elastic modulus was calculated from the linear portion of the stress-strain curve in Figure 27. At 191°C the average elastic modulus was 14.8 GPa for the [±45] fiber orientation.

The UTS and the modulus for the [0/90] specimens were considerably higher than those for the [±45] specimens. This is to be expected because for the [0/90] fiber orientation the material response is fiber-dominated and the matrix has little effect on the strength or stiffness of the material. In the case of the [±45] fiber orientation, the matrix has a strong influence on strength and stiffness hence the lower UTS and stiffness values obtained for the [±45] specimens. Ultimate Tensile Strength values for both [0/90] and [±45] fiber orientations are summarized in Table 6 for all prior aging conditions.

Table 6: Ultimate Tensile Stress for [±45] and [0/90] IM7/BMI 5250-4 with different prior aging times

Prior Aging Time (h)	[±45] UTS (MPa)	[0/90] UTS (MPa)
0	165	849
10	164	718
50	170	932
100	168	848
250	161	875
500	161	531
1000	154	683

Stiffness values obtained for both [0/90] and [±45] fiber orientations are presented in Table **7** for all prior aging conditions.

Table 7: Young's modulus for [±45] and [0/90] IM7/BMI 5250-4 specimens for different aging times

Prior Aging Time (h)	[±45] Young's Modulus (GPa)	[0/90] Young's Modulus (GPa)
0	14.8	60.9
10	14.5	75.1
50	14.9	59.1
100	15.1	63.9
250	15.9	54.4
500	17.1	76.6
1000	15.3	82.9

.

Tensile tests to failure allowed us to compare the differences between the tensile properties of the [±45] and the [0/90] fiber orientations and provided information on how prior aging affects the mechanical properties. Figure 28 shows the UTS as a function of prior aging time for both fiber orientations.

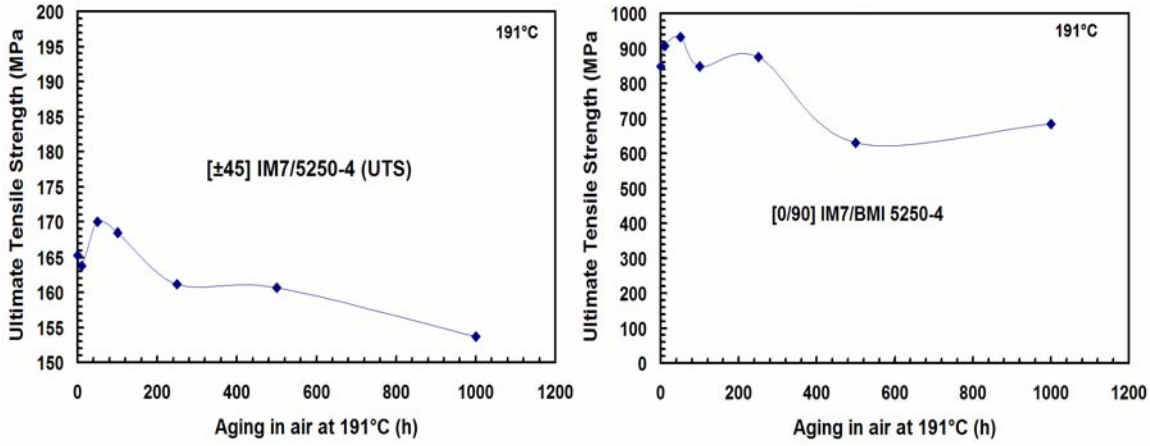

(a) **(b)**

Figure 28: UTS as a function of prior aging time spent in air at 191°C for (a) [±45] and (b) [0/90] fiber orientations

Results in Figure 28 show that the UTS decreases with increasing prior aging time. This is what we would expect because of the matrix degradation during the aging process. The matrix distributes the load between the fibers and as the matrix decays the UTS will decrease.

Failure of the Specimens

The specimen failure modes depend on the orientation of the fibers in the specimen. The [±45] specimens exhibited larger deformation due to "scissoring" of the fibers. A typical stress-strain curve for the [±45] fiber orientation is shown in Figure 29.

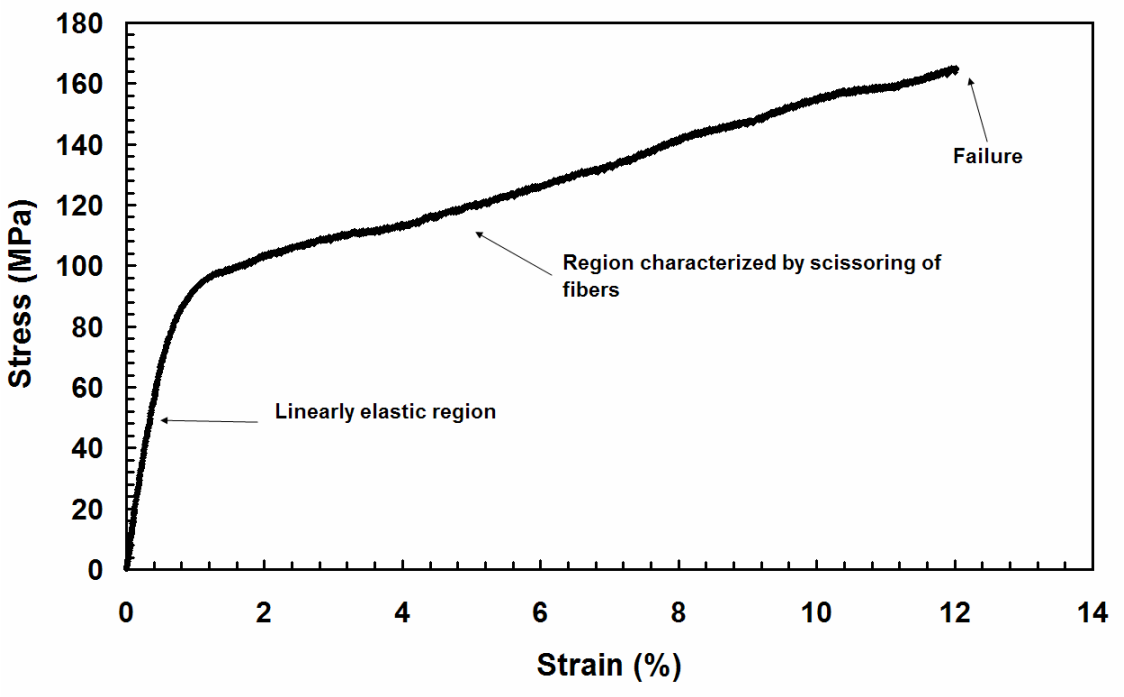

Figure 29: Stress vs strain for [±45] fiber orientation of BMI IM7/5250-4

The initial response of the [±45] specimen is nearly linear elastic. As the load increases the fibers begin to "scissor". The fibers detach from the edges of the composite and rotate toward the loading axis. This corresponds to the portion of the graph where the strain increases rapidly. The specimen breaks at approximately 45° angle to the loading direction. An illustration of a failed [±45] specimen is shown in Figure 30.

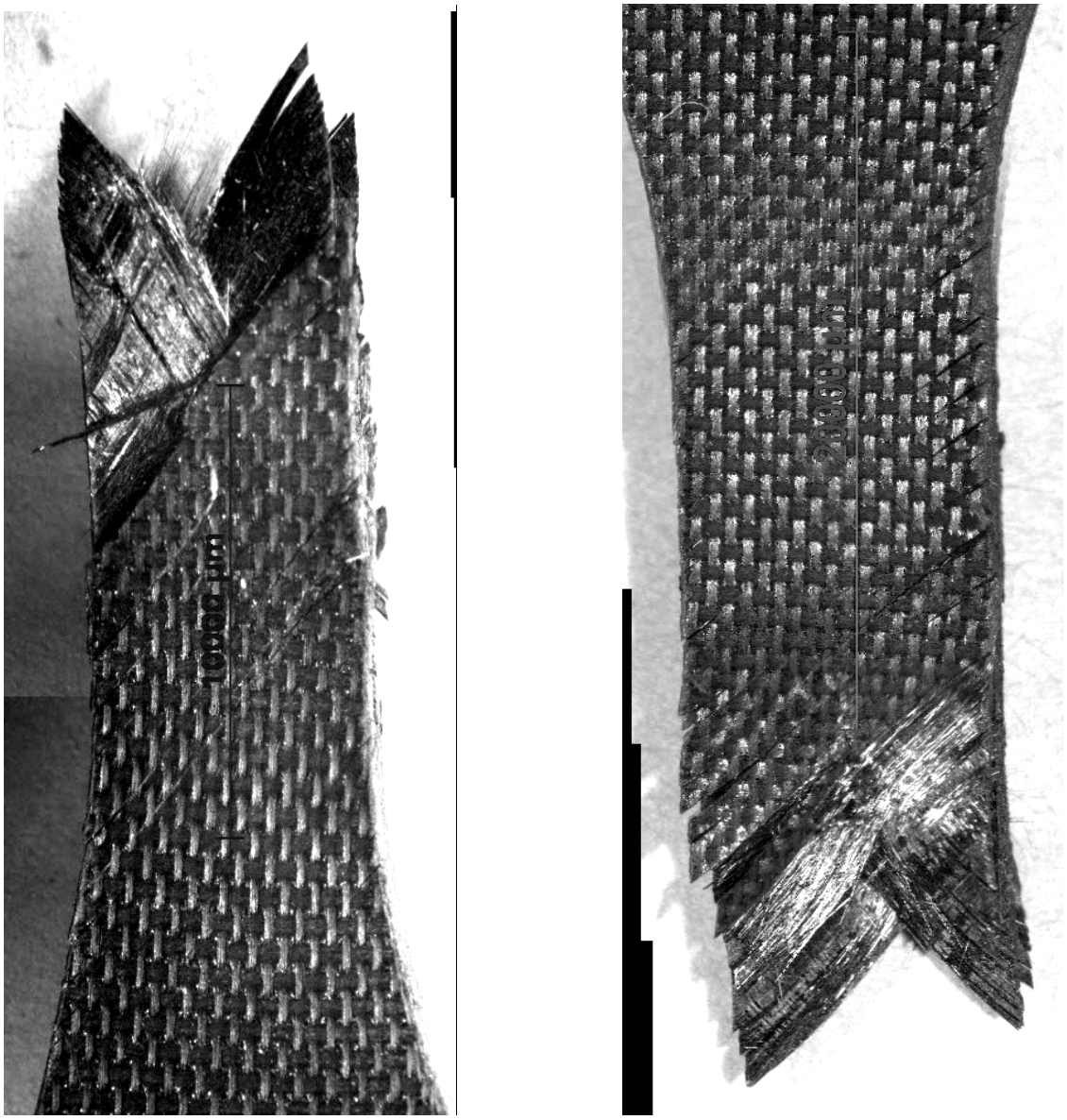

(a) (b)

Figure 30: Illustration of the bottom (a) and the top (b) of a [±45] IM7/BMI 5250-4 specimen showing fiber scissoring prior to failure

In the figure you can see that the failure occurs in the gage section of the specimen. There is very little fiber fracture noticeable in the picture. Failure is due to the fibers pulling away from the edge toward the loading axis and then failing when they cannot rotate anymore. Side views of the failed [±45] specimen are shown in Figure 31.

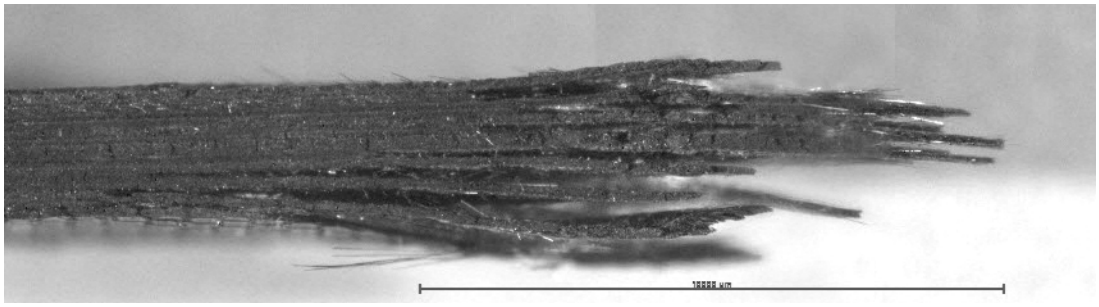

(a)

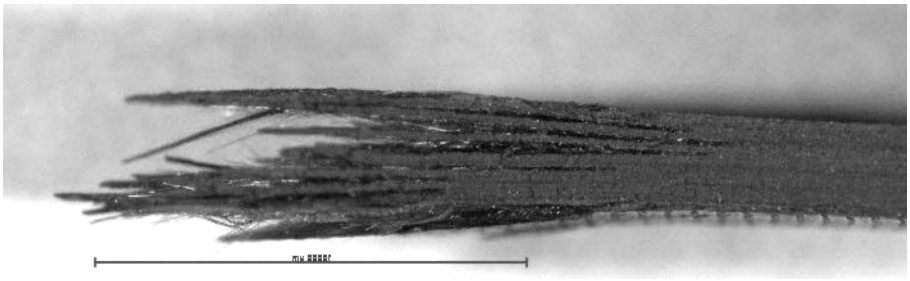

(b)

Figure 31: Side view of [±45] IM7/BMI 5250-4 specimen fractured in tensile testing showing delamination

The fibers in the [±45] specimen pull on the matrix as the fibers scissor and separate the lamina as the stress increases producing delamination.

The [0/90] specimens have a different stress-strain response and consequently a much different failure mode. In the [0/90] specimens the fibers dominate the material behavior, producing a stress-strain curve that is linear to failure as shown in Figure 32.

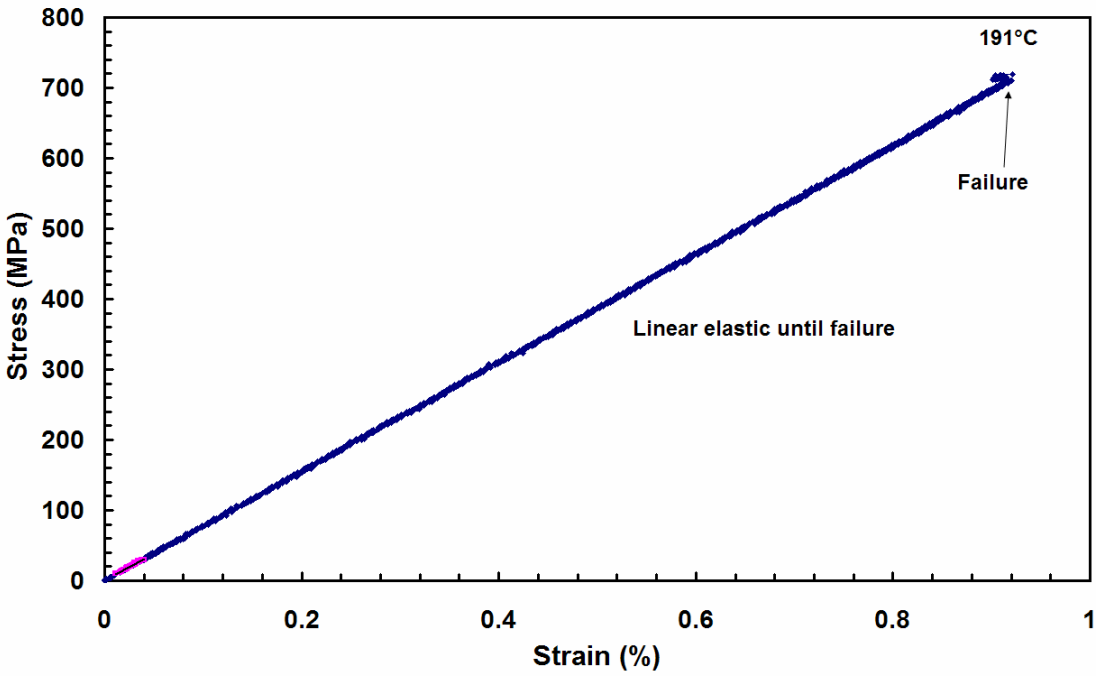

Figure 32: Stress vs strain curve for the [0/90] IM7/BMI 5250-4 specimen aged 10 hours illustrating linear behavior until failure

Figure 33 shows a failure surface of a [0/90] specimen. Both fracture and pull-out of the 0° fibers are observed.

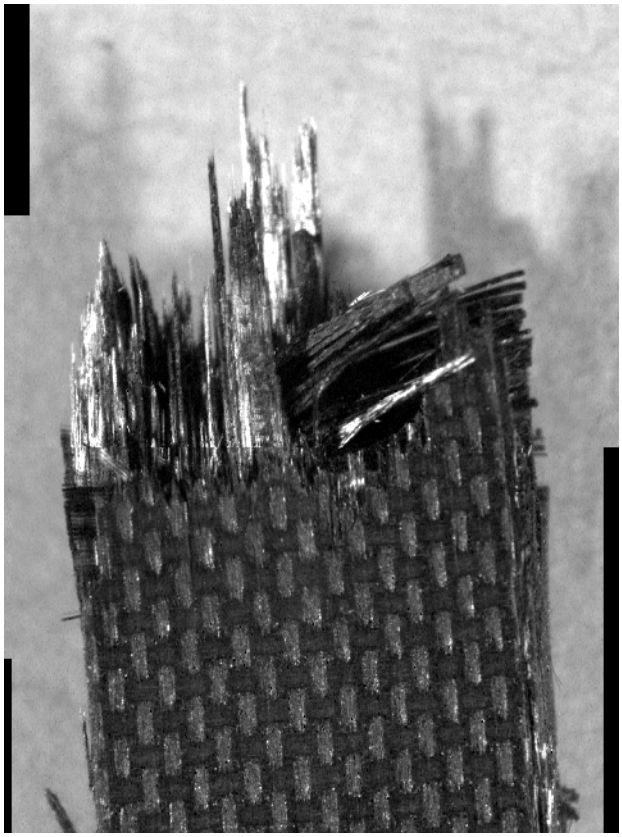

Figure 33 : Fracture surface of a [0/90] IM7/BMI 5250-4 specimen subjected to tensile loading demonstrating fiber fracture and fiber pull out after failure

Figure 34 shows an expanded view of the damage zone that includes the entire length of the specimen.

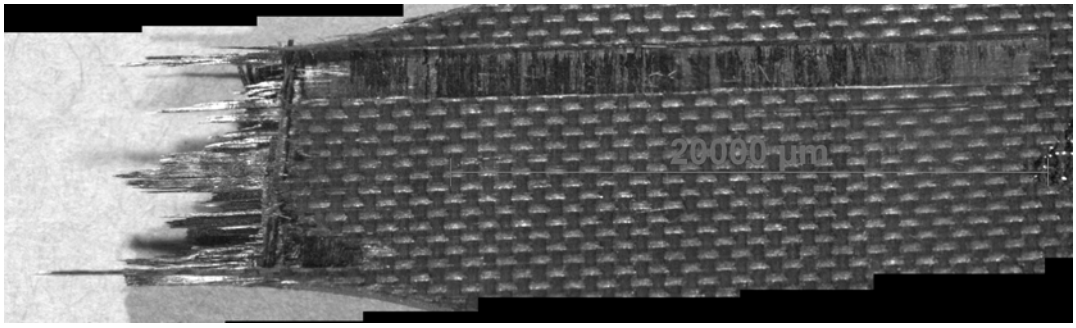

Figure 34: Expanded view of damage zone for [0/90] IM7/BMI 5250-4 subjected to tensile loading demonstrating fiber fracture and fiber pull out along entire length of the specimen

This extended damage zone is seen only in the [0/90] specimens. In the [±45] specimens the damage zone was confined to the gage section with some fibers pulling away from the matrix along the edge of the specimen. Again this is due to the fibers scissoring. The [0/90] specimens are loaded along the direction of the fibers. In this case failure occurs when the fibers reach their ultimate tensile strength. Because the load is being applied along the entire fiber uniformly not all of the fibers will break in the gage section. If there are weaker points due to processing the failure may occur art that point. This may be the cause of the extended damage zone for the [0/90] specimens.

Creep Tests on [±45] Specimens

Creep tests were conducted to determine the effects of prior aging on the creep behavior. The [±45] specimens were subjected to a near instantaneous load-up followed by a creep test. In the real world it is not possible to apply an instantaneous load, therefore a suitable load rate was chosen to load the specimen as quickly as possible while avoiding dynamic effects. The load was applied at a rate of 2 MPa/sec which resulted in a load-up time of 66 seconds.

Before loading the specimens are heated up to 191°C at a rate of 2°C/min and allowed to dwell at 191°C for thirty minutes. During the heat-up and the dwell period the specimens produced thermal strain. Thermal strain was approximately the same for all specimens tested. Only mechanical strain was considered in evaluation of results. Figure 35 shows the early portion of the load-up to creep stress for all creep tests.

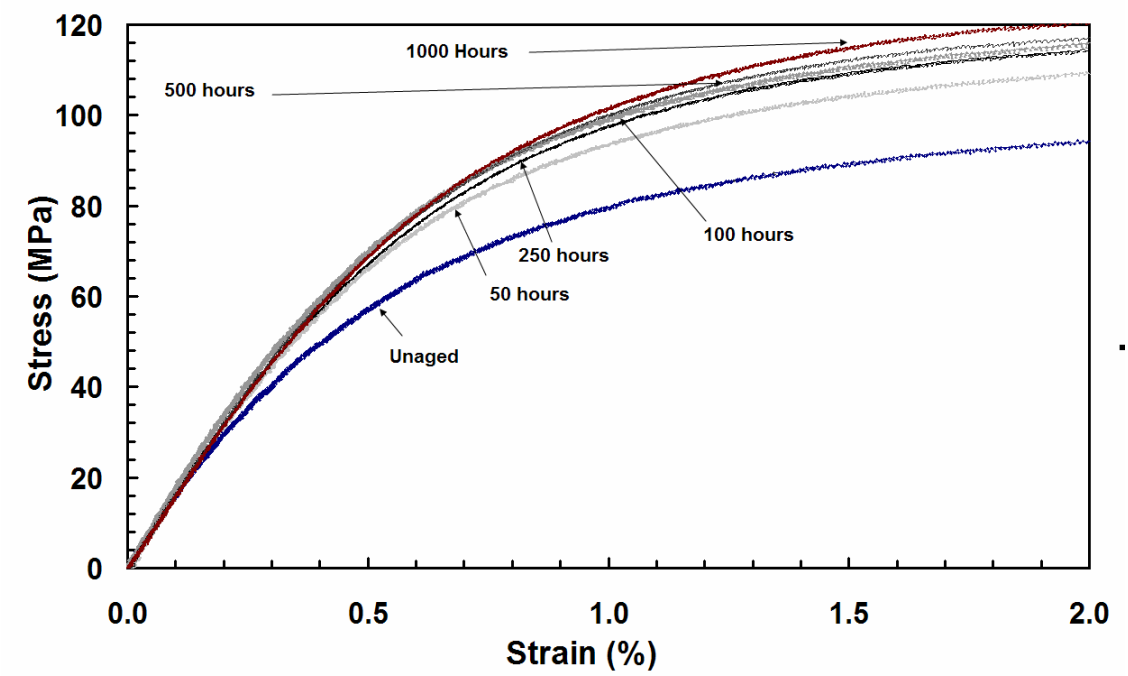

Figure 35: Early portions of the load-up stress-strain curves for all of the [±45] IM7/BMI 5250-4 subjected to creep tests. Increase in stiffness with increasing prior aging time is evident.

The graph shows that the stiffness of the composite increases with increasing prior aging time. Figure 36 shows the complete Stress vs Strain curve for all of the [±45] specimens subjected to creep tests.

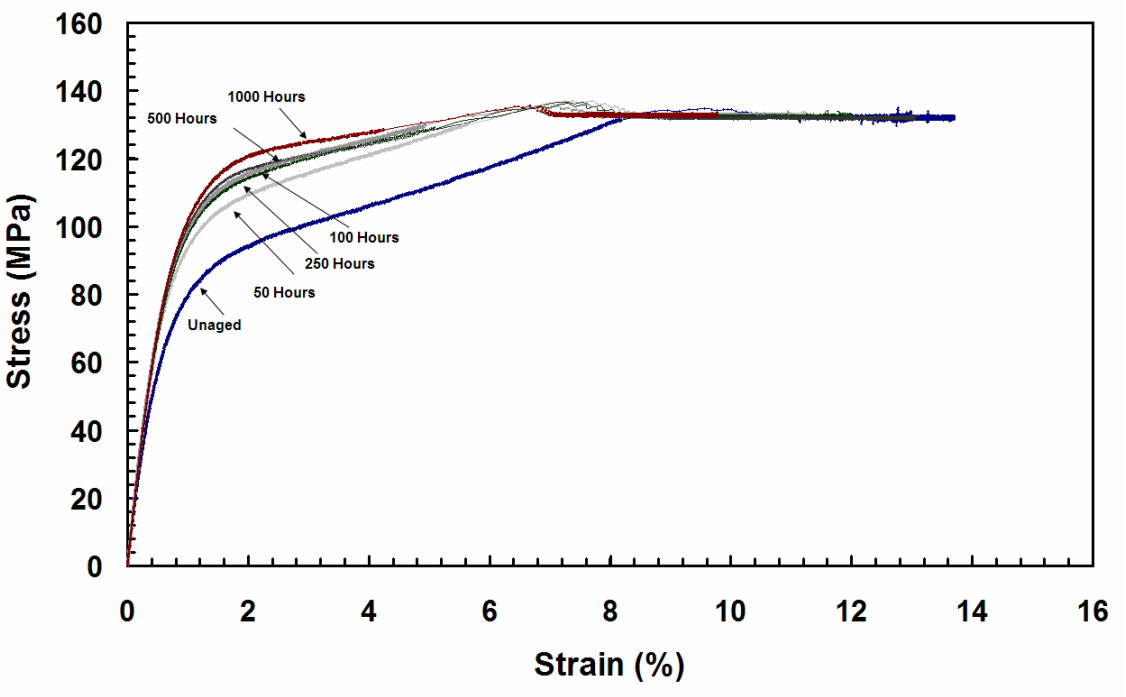

Figure 36: Complete Stress vs Strain curves for the [±45] IM7/BMI 5250-4 specimens showing the higher stiffness of the aged specimens

Specimen-to-specimen variation must be addressed before evaluating the creep strains. The Young's modulus varied for the different specimens in a given aging group, even though all specimens were cut from the same panel. In order to account for scatter due to specimen-to-specimen variation the creep strains, and the recovery strains, were adjusted using the following equation:

$$\varepsilon_{adj} = \frac{E}{E_{avg}}\varepsilon \tag{29}$$

where E_{avg} is the average Young's Modulus for each aging group of specimen. (37)

The modulus for each of the specimens subjected to creep tests was calculated using the stress-strain curve produced during the load-up to creep stress. The average modulus values for each aging group are given in Table 8.

Table 8: Average Young's modulus values for different aging groups

Prior Aging Time (h)	Average Modulus GPa
0	15.5
50	15.4
100	15.9
250	15.5
500	17.2
1000	16.5

Creep strain vs time curves obtained for specimens subjected to different prior aging times are shown in Figure 37.

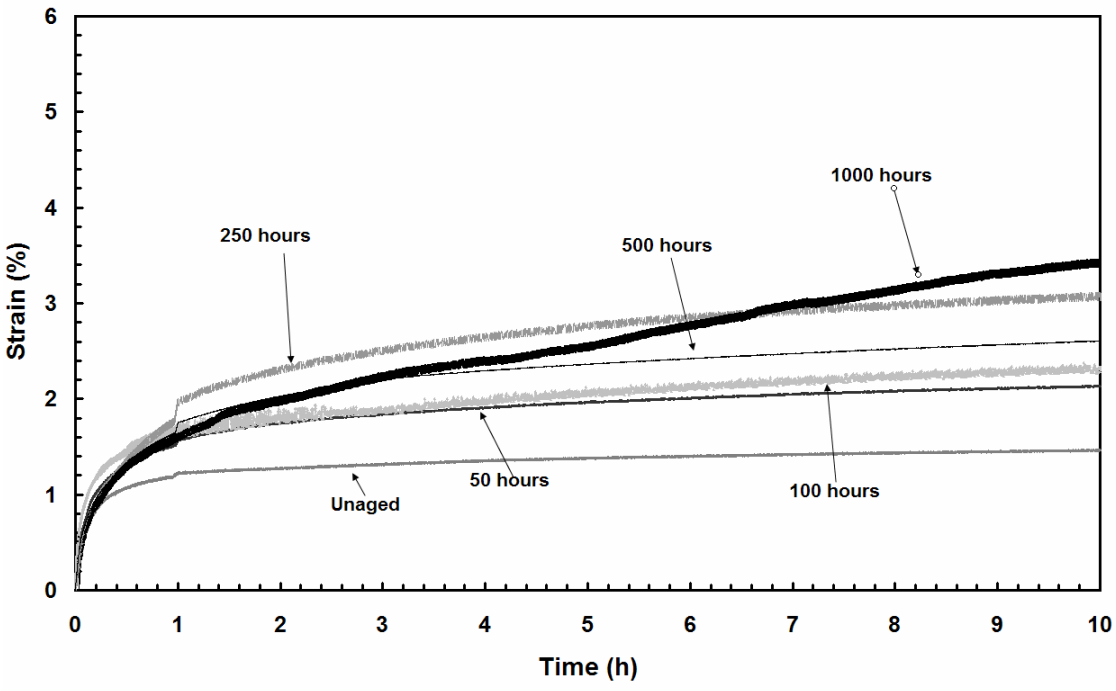

Figure 37: Creep Strain vs time for the [±45] specimens subjected to prior aging at 191°C in air

It is seen in Figure 37 that creep strain tends to increase with increasing prior aging time. The specimen aged for 250 hour was the only specimen to fail during the creep test. This failure could be attributed to a defect in the specimen.

Secondary Creep Rate

As was discussed earlier, specimens subjected to creep tests will undergo the initial primary creep regime where the creep rate decreases. Then the specimen will enter the secondary creep regime, where the creep rate remains constant. Then the specimen may reach the tertiary creep regime that is characterized by a sharp increase in creep rate and usually ends in failure.

The secondary creep rates for the [±45] specimens are shown in Figure 38.

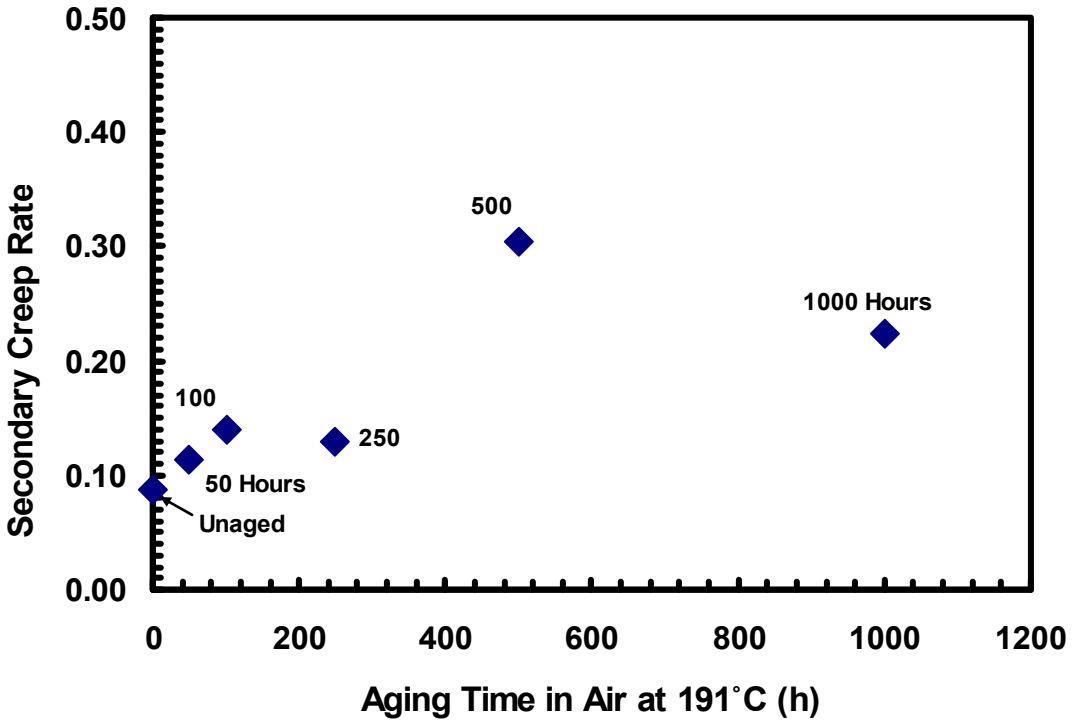

Figure 38: Secondary creep rates with respect to time spent aging in air at 191˚ C for [±45] IM7/BMI 5250-4 specimens subjected to creep tests at 80% UTS

The trend for the secondary creep rates is to increase with increasing prior aging time. This is what should be expected. The aging degrades the matrix which protects the fibers as well as helps distribute the load between the fibers. As the matrix cracks and decays, the fibers become destabilized and a higher creep rate results. The aged specimens will reach the maximum stress sooner and consequently fail sooner than specimens that are unaged.

Creep Tests on [0/90] Specimens

Because behavior of the [0/90] specimens is fiber dominated creep strains were negligible. The specimens were loaded up to creep stress level at a rate of 6 MPa/sec. The loading time was 74 seconds.

The [0/90] specimen accumulated less than 1% strain after 27 hours of creep. Most of this strain was accumulated during load-up. The specimen that was aged for 1000 h accumulated negligible creep strain.

Because of the negligible creep strains, creep tests were conducted only on the unaged [0/90] specimen and the [0/90] specimen aged for 1000 h, the two groups that could best illustrate the effect of prior aging time on creep. The results are shown in Figure 39.

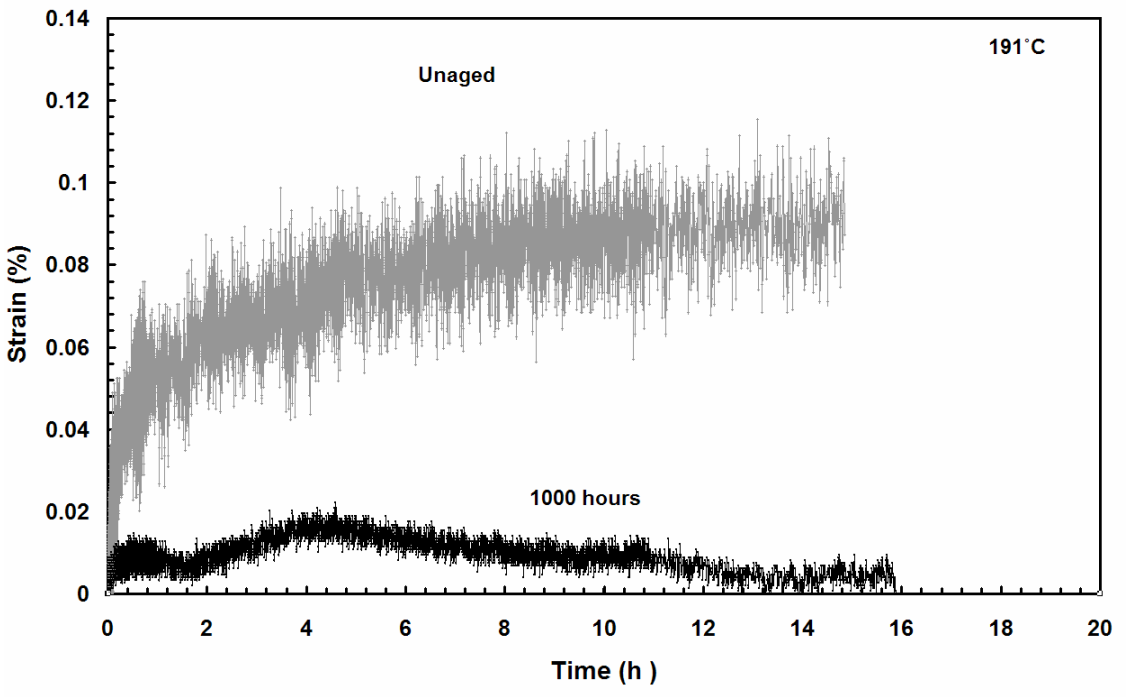

Figure 39: Creep strain vs time for [0/90] IM7/BMI 5250-4 unaged specimen and [0/90] specimen aged 1000 h

The graph in Figure 39 shows that the [0/90] specimens do not exhibit near the same amount of creep stain as the [±45] specimens do.

Recovery at Zero Stress

In the case of a purely elastic material when the load is removed the strain will return to zero. This is not the case when inelastic deformation is present. When loaded beyond the elastic limit most materials will exhibit some deformation after the load is removed. A complete creep-recovery test consists of a loading phase, the creep phase, unloading to zero stress and recovery. Figure 40 is a schematic that shows the different phases of the creep-recovery.

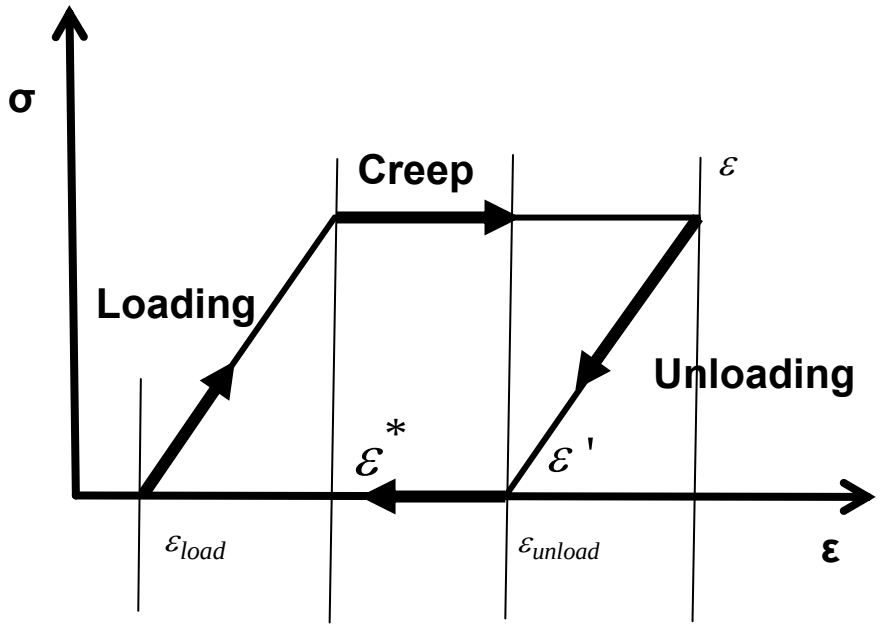

Figure 40: Schematic of a creep-recovery test to include loading, creep, unloading and recovery

Using the schematic in Figure 40 the percentage of total creep strain recovered can be found using the following equation

$$\varepsilon_R\% = \left(\frac{\varepsilon^* - \varepsilon'}{\varepsilon'} \right) * 100 \quad \textbf{(30)}$$

To determine the effects of prior aging on creep and recovery, creep-recovery tests were conducted on the unaged and the [±45] specimens. Figure 41 shows an entire creep test cycle for the unaged [±45] specimens and those aged for 1000 h. Figure 41 shows that the stress strain curves obtained from the creep recovery tests in specimens with different aging history are qualitatively similar

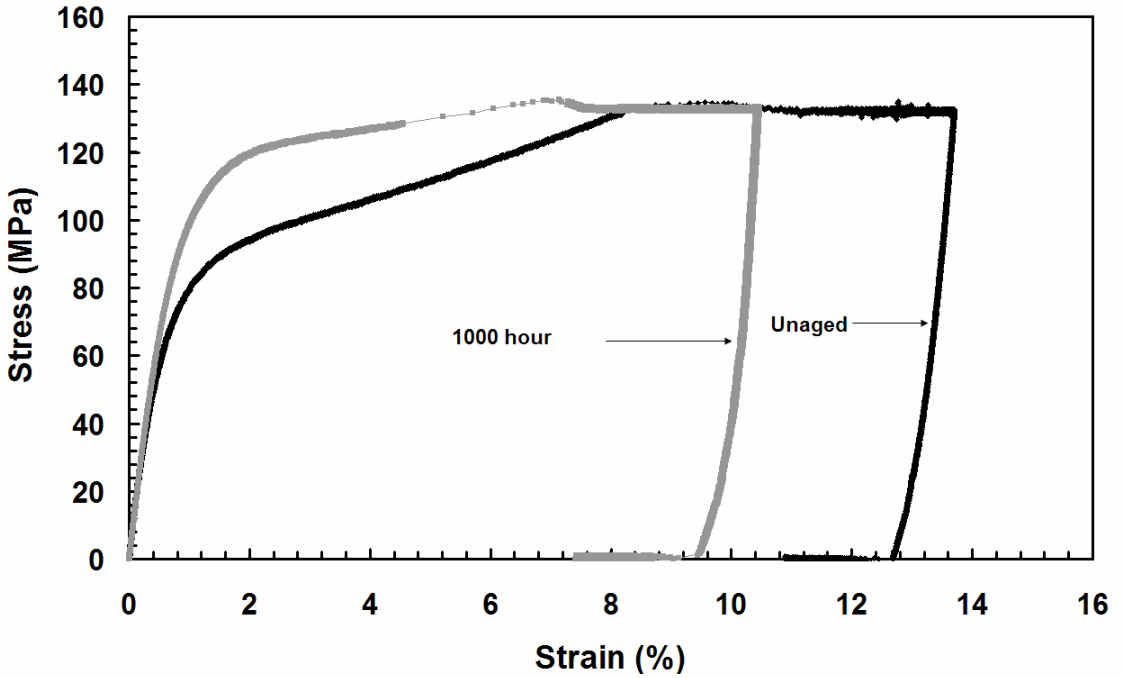

Figure 41: Stress-strain curves obtained in creep-recovery tests for unaged [±45] IM7/BMI 5250-4 specimens and specimens aged for 1000 h

Figure 42 shows the recovered strain as a function of time for both of the specimens.

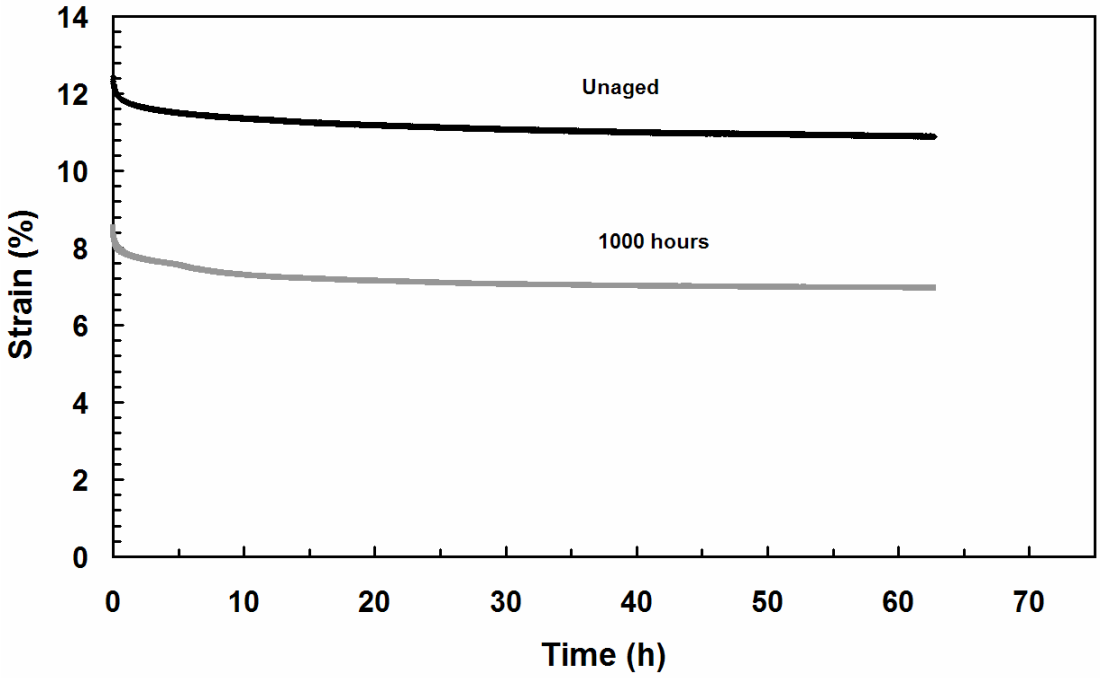

Figure 42: Recovered strain as a function of time for unaged [±45] IM7/BMI 5250-4 specimens and specimens aged for 1000 h

The rate at which the strain is recovered is almost identical for both specimens and they both appear to have leveled off asymptotically which would indicate that neither the unaged nor the aged specimen would achieve complete strain recovery even if they were allowed to recover for a longer period of time. This would suggest that permanent damage developed in both specimens during creep test.

Figure 43 shows the percentage of strain measured immediately upon reaching zero stress that was recovered by the two specimens. It is seen that the specimen that was aged for 1000 hours recovered almost 19% while the unaged specimen recovered 12.5% of the strain measured immediately upon reaching zero stress (Strain ε' in Figure 40).

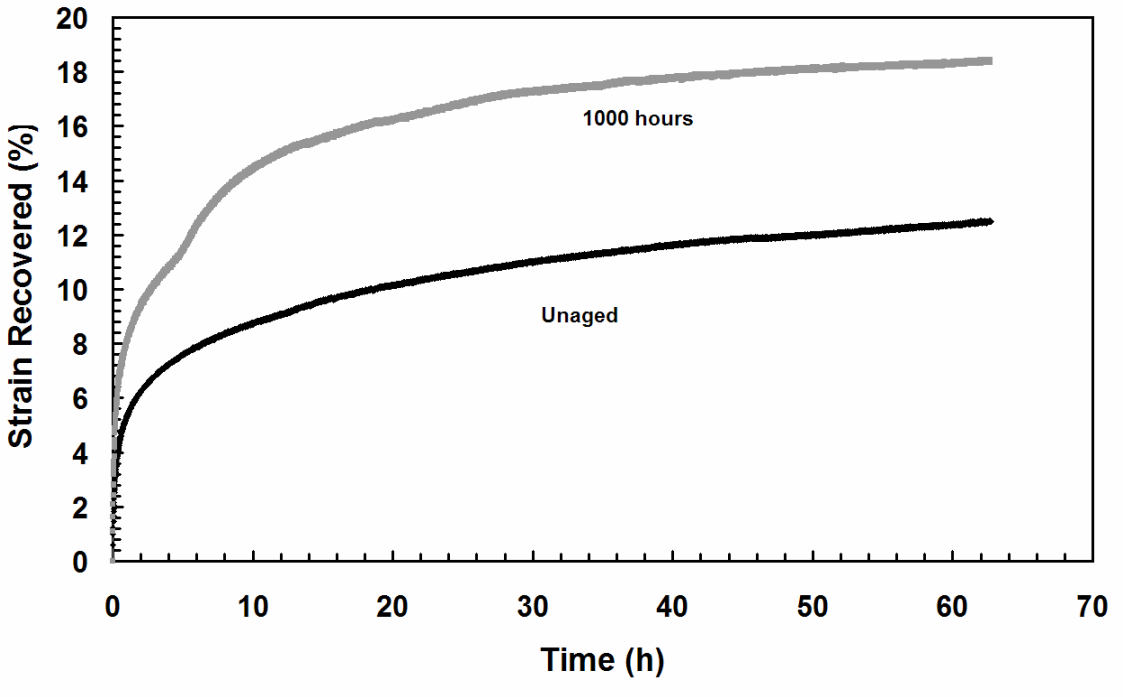

Figure 43: Percent strain recovered vs time for unaged [±45] IM7/BMI 5250-4 specimens and specimens aged for 1000 h

Figure 43 shows that the percent of creep strain recovery increases with increasing prior aging time.

VI. Concluding Remarks

This section will summarize the testing results and concluding remarks. This section will also address recommendations for follow on testing of the composite.

Concluding Remarks

The effects of aging on creep behavior of the BMI IM7/5250-4 composite were explored. Aging had a distinct effect on the weight of the specimens, their tensile properties and recovery response.

The specimens were aged for up to 1000 hours. The specimens that were aged for 1000 h lost a total of 1% of their as-received weight. Nearly one third of this weight loss occurred in the vacuum oven before the aging process began. The amount of weight lost solely due to aging differed between the [±45] fiber orientation and the [0/90] fiber orientations. The [0/90] fiber orientations lost 0.64% of the initial weight and the [±45] fiber orientation lost 0.72% of the initial weight. The majority of the weight loss occurred in the first 24 hours of aging, weight loss continued until the 1000 hours but at a much slower rate than the initial 24 hours. This weight loss is attributed to the degradation of the matrix in the composite.

The difference in weight loss between the different fiber orientations is attributed to the number of entryways on the side of the matrix that allows for environment to more readily enter the composite. The [±45] fiber orientation has more of these openings and therefore loses more weight in a given amount of time.

The specimens, aged and unaged, were subjected to tensile tests to failure to evaluate the effect that prior aging had on tensile properties. It was shown that the UTS of the composite decreased with an increase in prior aging time in air at 191°C. The elastic modulus increased with prior aging time. The stress-strain curve of the 1000 h aged specimen is notably steeper than that of the unaged specimen. This can be attributed to the aged specimen having less matrix to absorb the load and transfer it between the fibers. The load is applied more directly to the fibers resulting in a stiffer composite. The aged specimens also exhibit lower failure strain.

Creep tests were conducted on the specimens to evaluate the effects of prior aging on the creep response. The [0/90] specimens did not exhibit large amounts of creep strain because the composite response was fiber dominant in tensile tests. The majority of the strain data were collected from the creep tests on the [±45] specimens.

The unaged [±45] specimen and the [±45] specimen aged for 1000 hours were also subjected to 60 h recovery at zero stress after a 100 h creep test. The recovery test showed that the unaged specimen recovered 12.5% while the aged specimen recovered almost 19% of the strain measured immediately after reaching zero stress. It should be noted that both of the specimens, aged and unaged, experienced permanent damage and are unlikely to reach full recovery even if the recovery time was much longer than 60 h.

Recommendations

The main focus of this study was to determine the effects of aging on IM7/BMI 5250-4 composite. A recommendation would be to age the material for longer periods of time to see a greater decay of the matrix and to assess how long it takes for the overall composite to be seriously affected. Another recommendation is to conduct creep tests of longer duration to assess if long term behavior can be predicted from short term creep data. Conduct creep-recovery experiments of longer duration to assess where the recovery saturates and how much permanent damage occurred. And finally it was discussed how modeling can predict behavior of viscoelastic materials. Characterize and apply a viscoelastic model to see if the behavior of IM7/BMI 5250-4 composites can be accurately predicted.

Bibliography

1. Kroschwitz, Jacqueline I. *Concise Encyclopedia of Polymer Science and Engineering* John Wiley & Sons 1990

2. Le Coustemer, P *Aging of Carbon-Fiber Reinforced Bismaleimide matrix composites in oxidative conditions* Composites Science and Technology 52 (1994) 433-437

3. Fox, Bronwyn *Investigation of Failure mechanisms in aged aerospace composites* Engineering Failure Analysis 11 (2004) 235-241

4. Kong, ESW; Lee, SM; and Nelson HG *Physical Aging in Graphite/Epoxy Composites* Polymer Composites 3 (1982) 29-33

5. Hill, Frederick Thomas. *The Materials of Aircraft Construction.* Sixth Edition. Sir Isaac Pitman & Sons, LTD, 1944

6. Berthelot, Jean-Marie. *Composite Materials Mechanical Behavior and Structural Analysis.* Springer-Verlag New York, Inc, 1999

7. Green, John A.S. and others. *New Materials for Next Generation Commercial Transports*. Washington DC, The National Academies Press, 1996.

8. Flower, Harvey M. *High Performance Materials in Aerospace.* First Edition. Chapman & Hall, 1995

9. Morawetz, Herbert. *Polymers the Origins and Growth of a Science* John Wiley and Sons 1985

10. Seymour, Raymond B. and Kirshenbaum, Gerald S. *High Performance Polymers: Their Origin and Development* Elsevier Science Publishing Co 1986

11. Birtles, Philip. *Boeing 777 Jetliner for a new century.* MBI Publishing Company 1998

12. Aronstein, David C., Hirschberg, Michael J. and Piccirillo, Albert C. *Advanced Tactical Fighter to F-22 Raptor: Origins of the 21st Century Air Dominance Fighter.* American Institute of Aeronautics and Astronautics 1998

13. Seymour, Raymond B. *Polymers for Engineering Applications* ASM International 1987

14. Riande, Evaristo and others. *Polymer Viscoelasticity: Stress and Strain in Practice.* Marcel Dekker, Inc, 2000.

15. Cytec Engineered Materials. "CYCOM 5250-4 RTM Resin System." http://www.cytec.com/business/EngineeredMaterials/Datasheets/CYCOM%20RTM%205250-4.pdf.

16. McCrum, N.G., Buckley, C.P., and Bucknall, C.B. *Principles of Polymer Engineering* Oxford University Press 1988

17. Donnet, Jean-Baptiste, and Bansal, Roop Chand. *Carbon Fibers* Marcel Dekker, Inc 1990

18. Electronic Development Labs *Plastic Dictionary* http://www.edl-inc.com/Plastic%20dictionary.htm

19. Mallick, P.K. *Fiber-reinforced Composites Materials, Manufacturing, and Design Second edition.* Marcel Dekker Inc, 1993

20. Daniel, Isaac M. and Ori Ishai. *Engineering Mechanics of Composite Materials.* Oxford University Press, 1994.

21. Ferry, John D. *Viscoelastic Properties of Polymers 3rd edition* John Wiley and Sons Inc. 1980

22. Christensen, R.M. *Theory of Viscoelasticity an Introduction 2nd edition* Academic Press, Inc. 1982

23. Findley, William N. and others. *Creep and Relaxation of Nonlinear Viscoelastic Materials.* North Holland Publishing Company, 1976.

24. Boyle, J.T. and Spence, J. *Stress Analysis for Creep* Butterworth & Co Ltd. 1983

25. Flugge, Wilhelm *Viscoelasticity 2nd edition* Springer-Verlag 1975

26. Aklonis, John J. and MacKnight, William J. *Introduction to Polymer Viscoelasticity.* 2nd edition. John Wiley and Sons, 1983

27. Hexcel Corporation *Prepreg Technology. Publication No. FGU 017b* March 2005

28. MTS Systems Corporation. *Model 793.00 System Software: User Information and Software Reference.* MTS Systems Corporation, 2001.

29. MTS Systems Corporation *Series 647 Hydraulic Wedge Grips Product Information; 100-027-131 E.* MTS Systems Corporation, February 2003

30. MTS Systems Corporation. *Reference Manual: Product Manual, High Temp/Axial Extensometers, 632.5;* MTS Systems Corporation, 1995.

31. MTS Systems Corporation. *Model 653 High-Temperature Furnaces Product Information; 015-059-101 F.* MTS Systems Corporation, 1995.

32. Pagano, N.J., Schoeppner, G.A., Kim, R. and Abrams, F.L. *Steady State Cracking and Edge Effects in Thermo-mechanical Transverse Cracking of Crossply Laminates.* February 1998

33. Baker, Alan and others. *Composite Materials for Aircraft Structures* (2nd Edition). American Institute of Aeronautics and Astronautics, Inc, 2004.

34. Day, Dwayne A. *US Centennial of Flight Commission; Composites and Advanced Materials* http://www.centennialofflight.gov /essay/ Evolution_of_Technology /composites/Tech40.htm

35. Schoeppner, GA, Tandon, GP, Ripberger, ER *Anisotropic oxidation and weight loss in PMR-15 composites* Science Direct Composites Part A 38 (2007) 890-904

36. Griffiths, Bob *High Performance Composites; Boeing sets pace for composite usage in large civil aircraft* May 2005 http://www.compositesworld.com/hpc/issues/2005/May/865/3

37. Ruggles-Wrenn, M.B. Advisor Notes. Air Force Institute of Technology, Wright- Patterson AFB OH, November 2005.

Appendix A
Photographs of Specimens

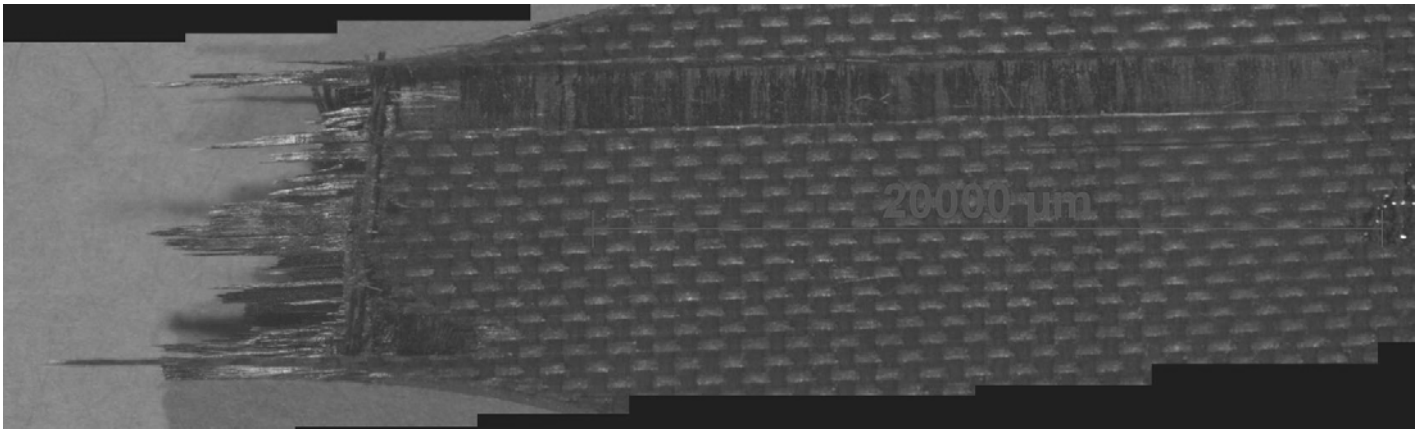

Figure 43 The top left side of a [0/90] IM7/BMI 5250-4 specimen showing the elongated damage zone due to fiber fracture and fiber pullout when subjected to tensile loads at 191°C

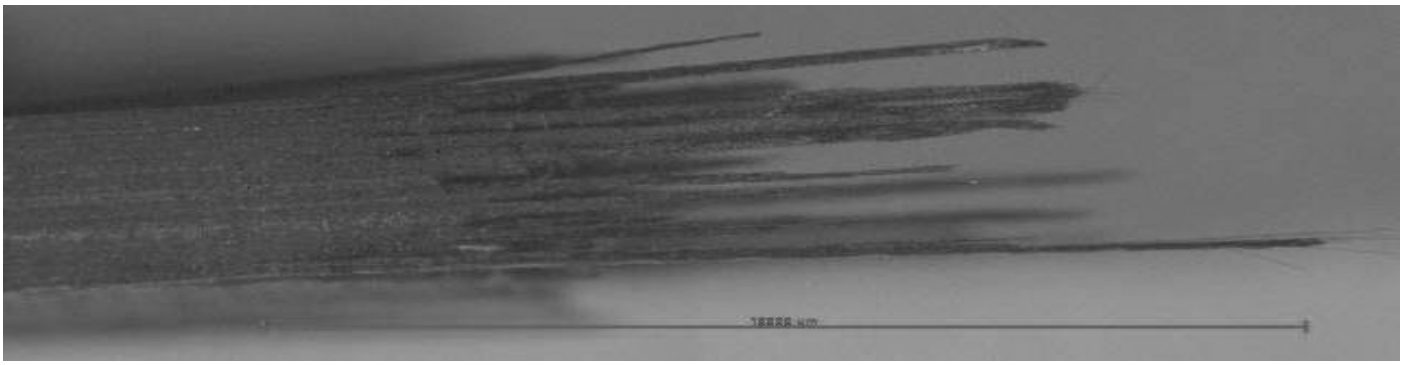

Figure 44: The top front portion of a [0/90] IM7/BMI 5250-4 specimen showing fiber pullout when subjected to tensile loads to failure at 191°C

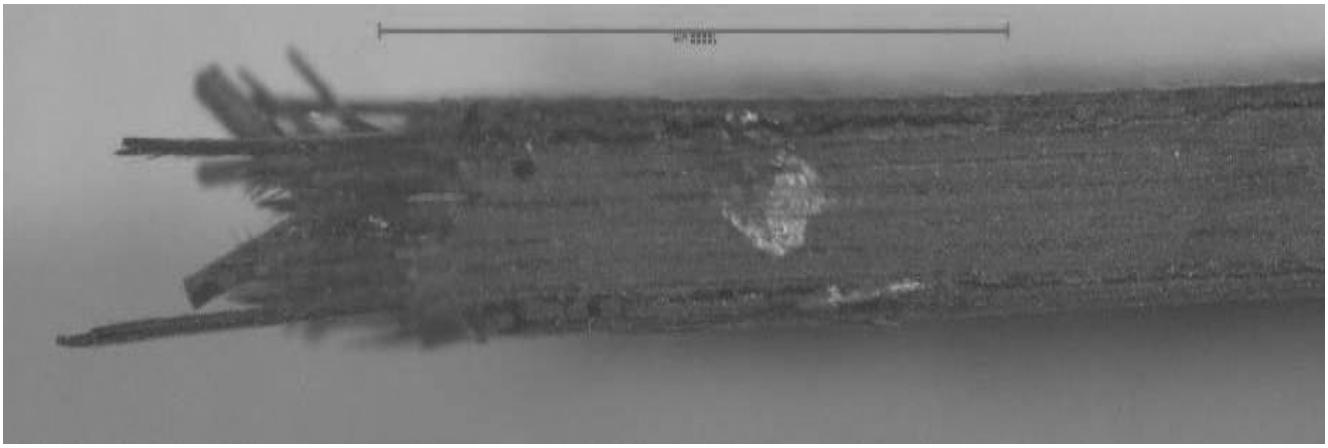

Figure 44 the bottom front portion of a [0/90] IM7/BMI 5250-4 specimen showing cracks in the matrix when subjected to tensile loads to failure at 191°C

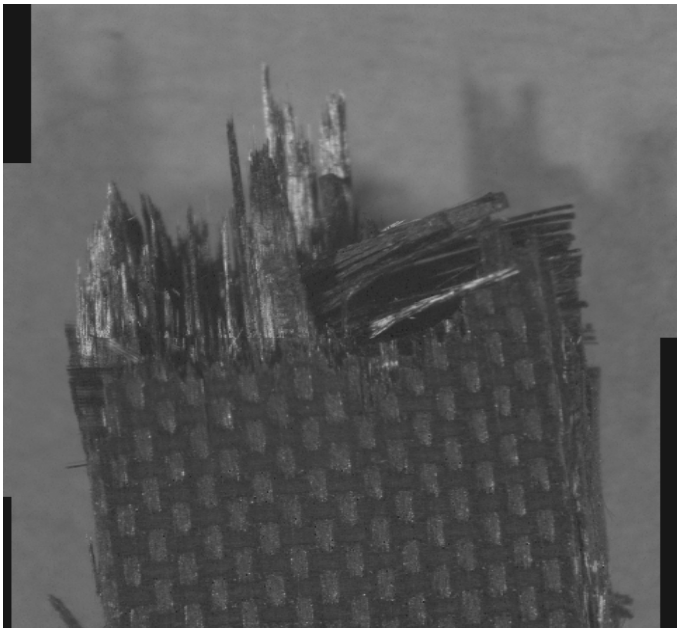

Figure 45: the bottom left side of the [0/90] IM7/ BMI 5250-4 specimen showing a close up view of the fiber fracture and pull out when subjected to tensile load to failure at 191°C

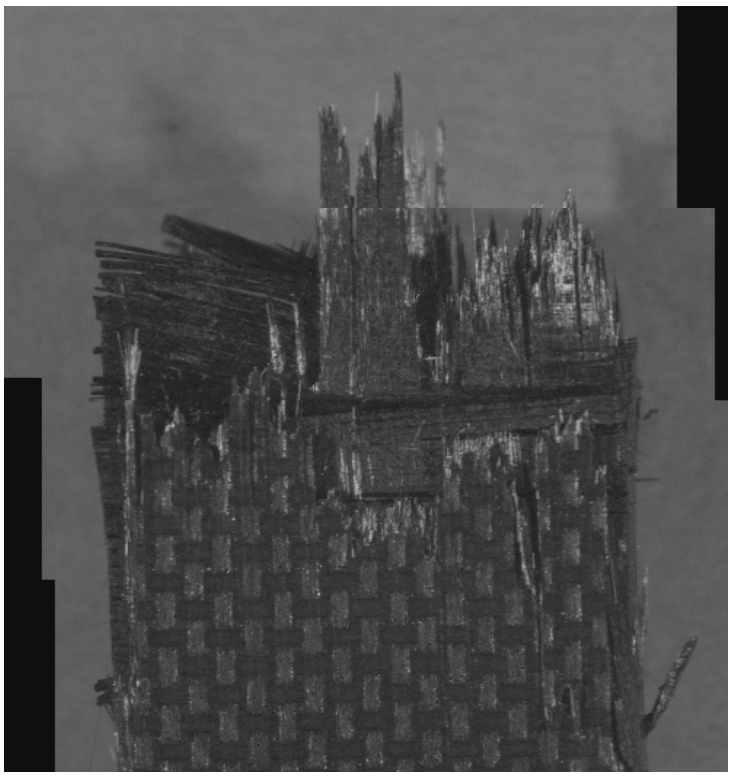

Figure 46: the bottom right side of the [0/90] IM7/ BMI 5250-4 specimen showing a close up view of the fiber fracture and pull out when subjected to tensile load to failure at 191°C

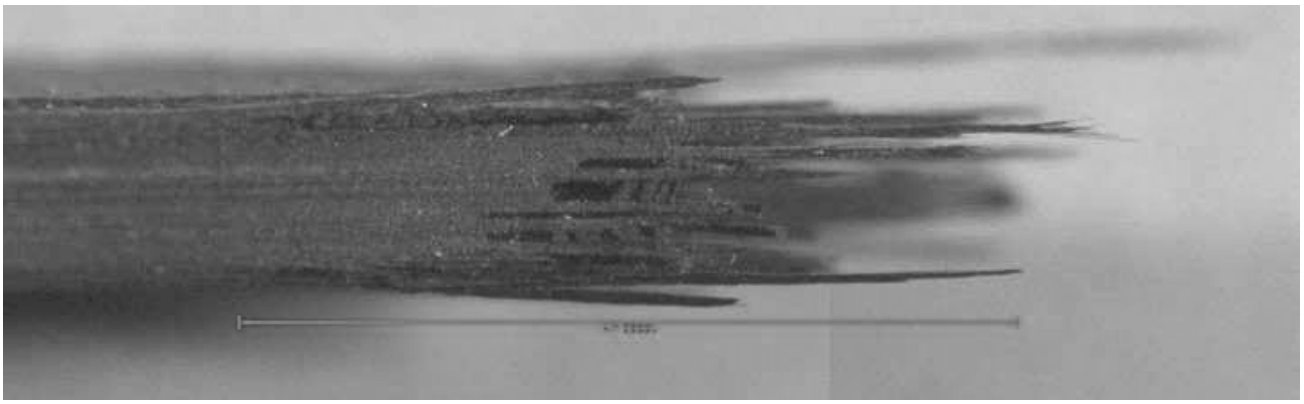

Figure 47: The top back side of the [0/90] IM7/ BMI 5250-4 specimen showing a close up view of the fiber fracture and pull out when subjected to tensile load to failure at 191°C

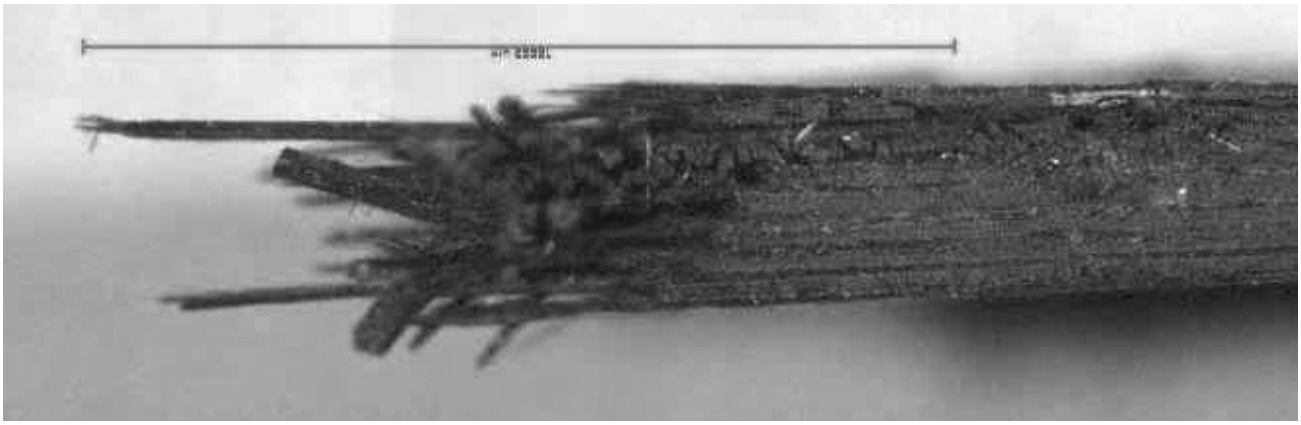

Figure 48: The bottom back side of the [0/90] IM7/ BMI 5250-4 specimen showing a close up view of the fiber fracture and pull out when subjected to tensile load to failure at 191°C

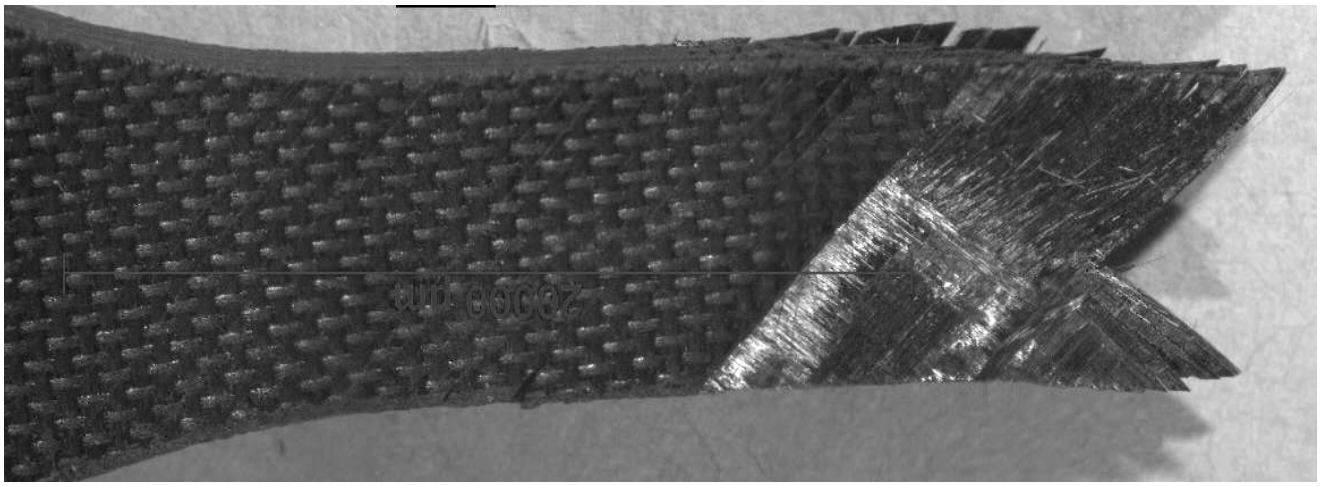

Figure 49: Top Left of the IM7/BMI 5250-4 [±45] specimens showing the angle of fracture due to the "scissoring" of the fibers when subjected to tensile load to failure at 191°C

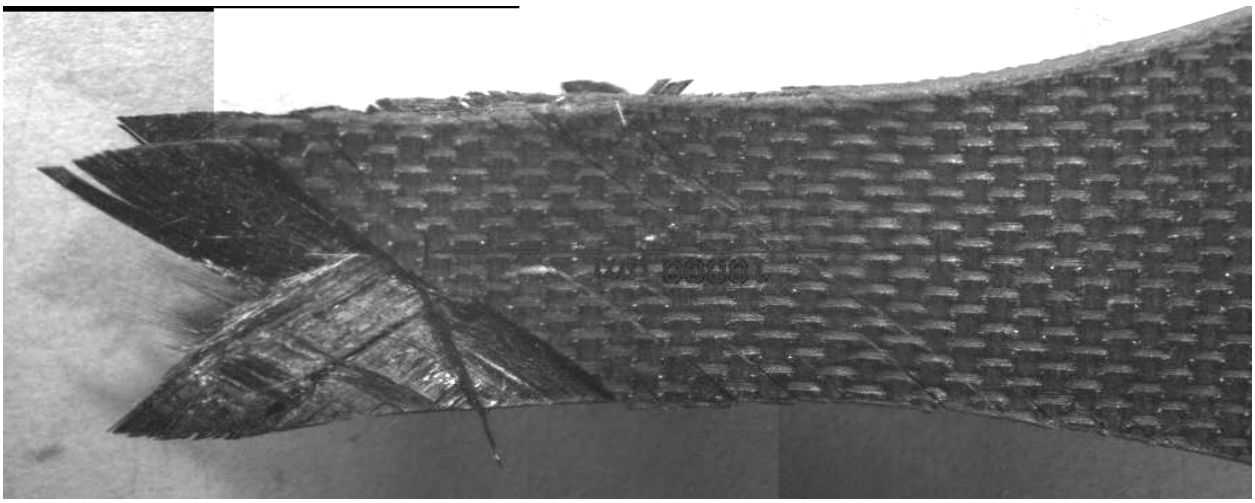

Figure 50: Bottom Left portion of the IM7/BMI 5250-4 [±45] specimens showing the angle of fracture due to the "scissoring" of the fibers when subjected to tensile load to failure at 191°C. Also notice the fibers pulling away from the sides of the composite as they rotate inward toward the loading axis

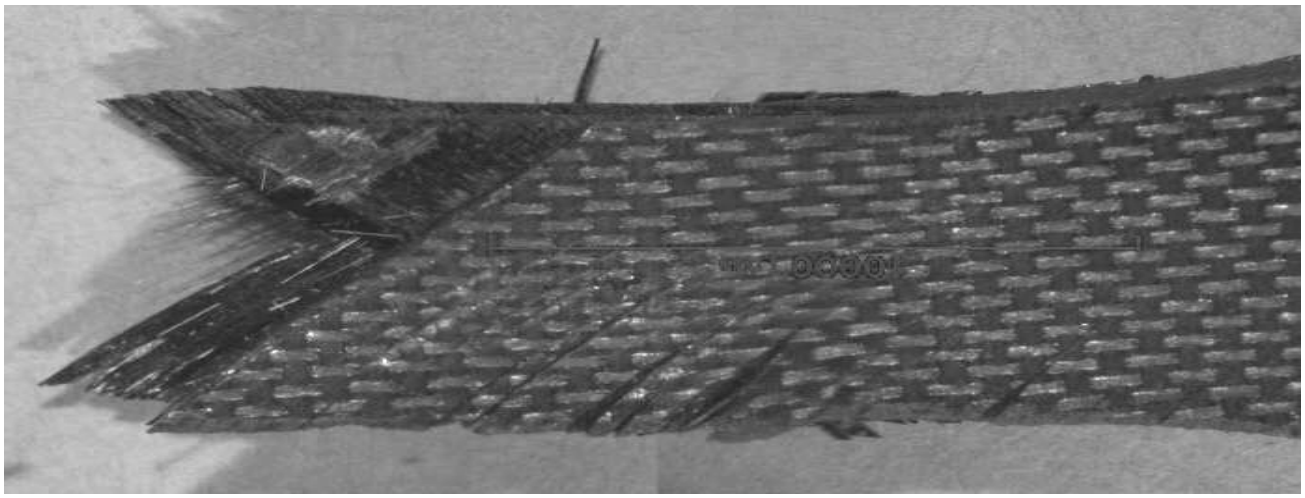

Figure 51: The top right portion of the IM7/BMI 5250-4 [±45] specimens showing the angle of fracture due to the "scissoring" of the fibers when subjected to tensile load to failure at 191°C. Also notice the fibers pulling away from the sides of the composite as they rotate inward toward the loading axis

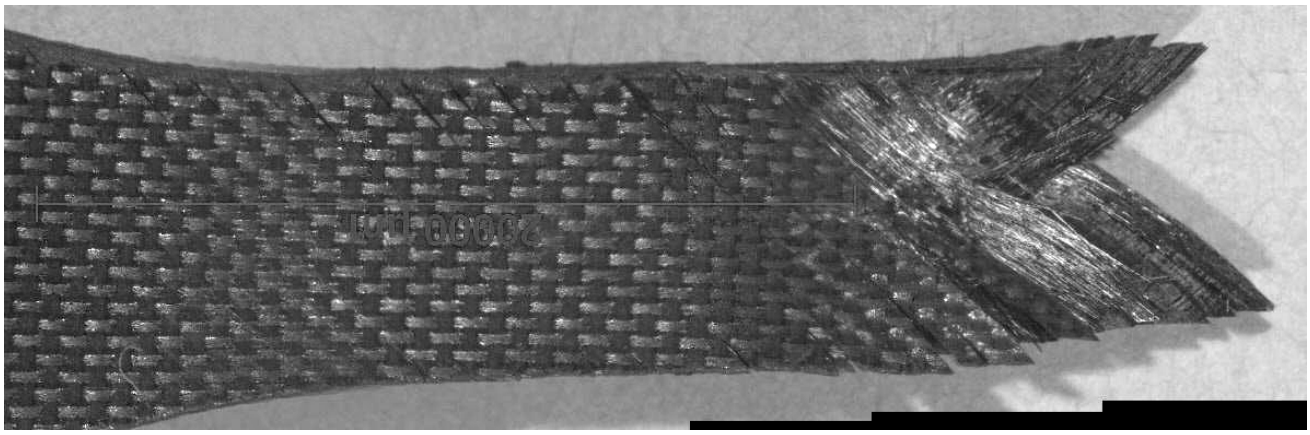

Figure 52: Bottom right portion of the IM7/BMI 5250-4 [±45] specimens showing the angle of fracture due to the “scissoring” of the fibers when subjected to tensile load to failure at 191°C. Also notice the fibers pulling away from the sides of the composite as they rotate inward toward the

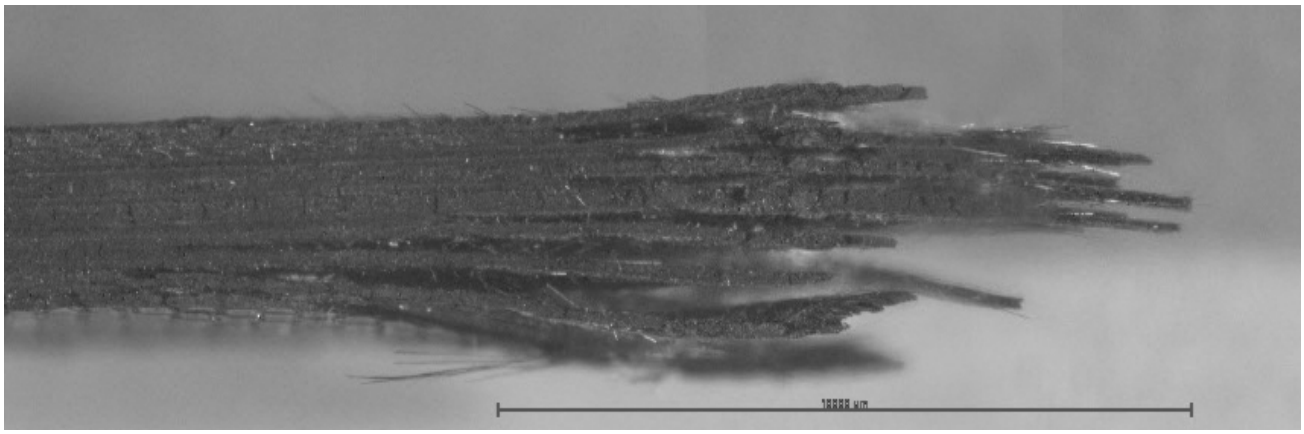

Figure 53: The top front portion of the IM7/BMI 5250-4 [±45] specimens showing the fibers pulling away from the sides of the composite when subjected to a tensile load to failure at 191°C

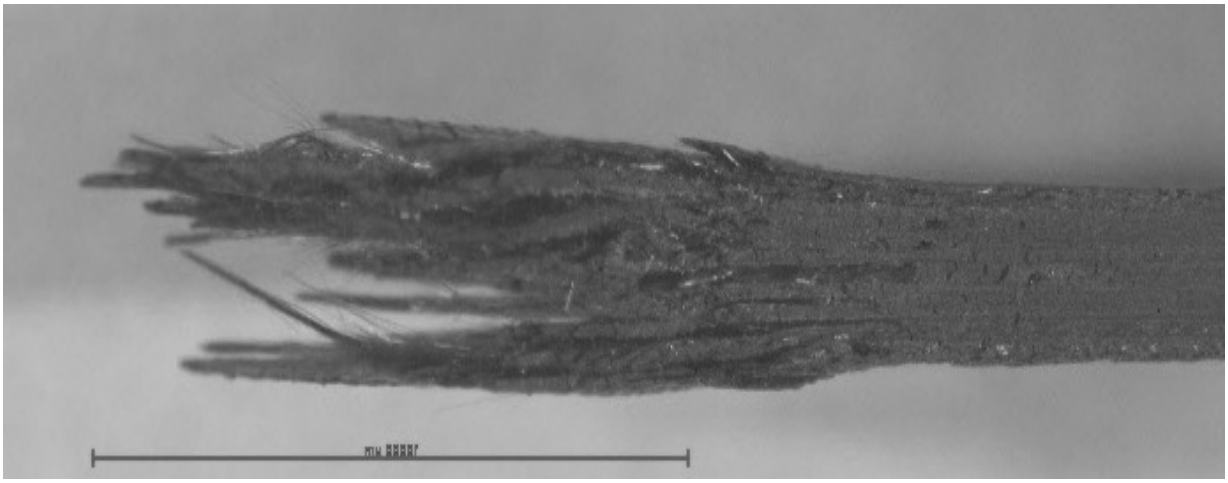

Figure 54: The top back portion of the IM7/BMI 5250-4 [±45] specimens showing the fibers pulling away from the sides of the composite when subjected to a tensile load to failure at 191°C

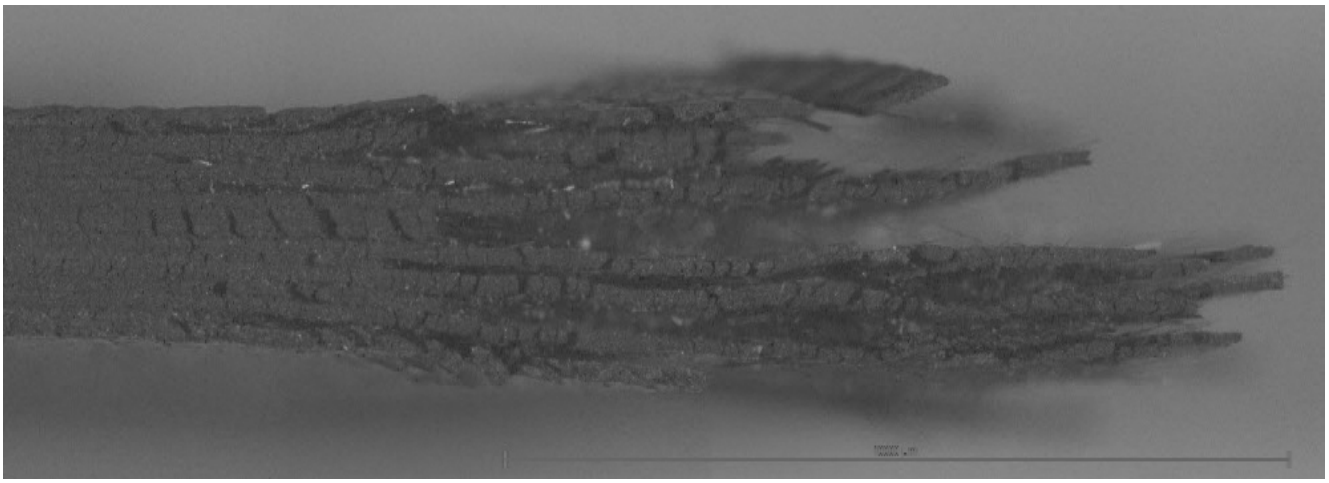

Figure 55: The bottom front portion of the IM7/BMI 5250-4 [±45] specimens showing the fibers pulling away from the sides of the composite and significant matrix cracking when subjected to a tensile load to failure at 191°C

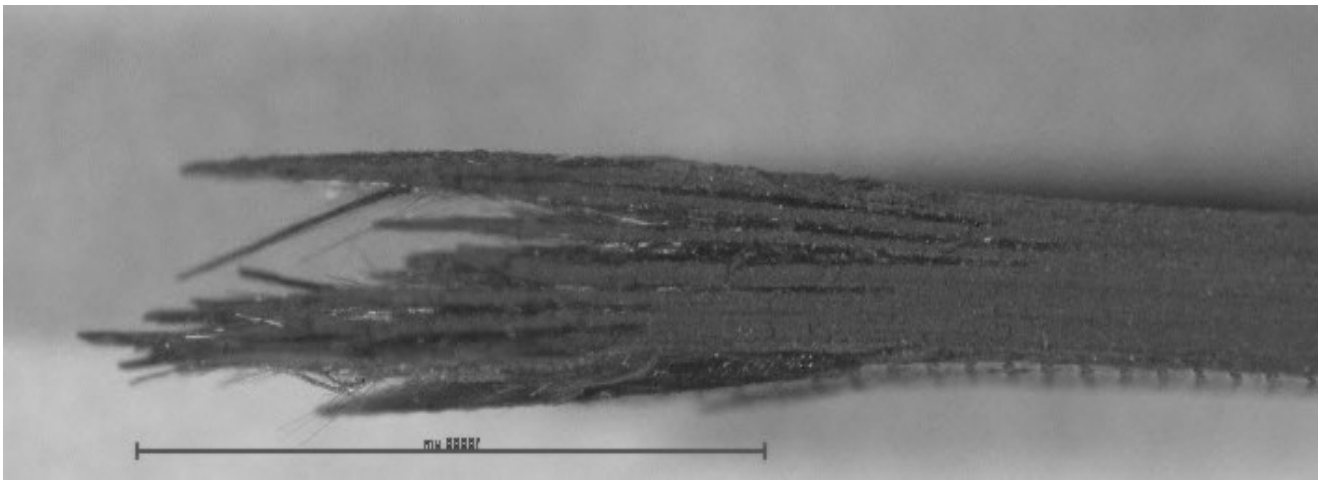

Figure 56: The bottom back portion of the IM7/BMI 5250-4 [±45] specimens showing the fibers pulling away from the sides of the composite and significant matrix cracking when subjected to a tensile load to failure at 191°C

Vita

Lieutenant Commander Robert A Salvia graduated from Saint Louis University High School in St. Louis Missouri. He entered undergraduate studies at The University of Texas in Austin, Texas where he graduated with a Bachelor of Science in Aeronautical Engineering in May 1996. He was commissioned into the United States Navy through the NROTC program at the University of Texas.

After being designated a Naval Flight Officer in October 1997, he was assigned to Patrol Squadron Thirty (VP-30) for Fleet Replacement Training in the Maritime Patrol and Reconnaissance Aircraft, the P-3C Orion, training in Anti-Submarine Warfare, and Intelligence Surveillance and Reconnaissance. Upon completion, he was ordered to his first fleet squadron, Patrol, Squadron Forty-Seven (VP-47) "The Golden Swordsmen." He deployed to Seventh Fleet in Japan in 1999 and to Fifth Fleet in the Persian Gulf in 2001. In January of 2002, he was transferred to Patrol Squadron Thirty (VP-30) where he was an Instructor Navigator and Tactical Coordinator in the P-3C Orion. In August of 2004 he was transferred to U. S. Forces Central Command, U. S. Fifth Fleet where he served as the Executive Assistant to the Fifth Fleet Operations Officer during Operation Iraqi Freedom. In August of 2005 he entered the Graduate School of Engineering and Management, Air Force Institute of Technology. Upon Graduation, he will be returning to the Fleet as a Department Head in Jacksonville, FL at Patrol Squadron Five (VP-5), "The Madfoxes."

REPORT DOCUMENTATION PAGE

Form Approved
OMB No. 074-0188

1. REPORT DATE *(DD-MM-YYYY)*	**2. REPORT TYPE**	**3. DATES COVERED** *(From – To)*
14-06-2007	Master's Thesis	Sept 05 – Jun 07

4. TITLE AND SUBTITLE

Effects of prior aging at 191°C on creep response of IM7/BMI 5250-4

5a. CONTRACT NUMBER

5b. GRANT NUMBER

5c. PROGRAM ELEMENT NUMBER

6. AUTHOR(S)

Salvia, Robert, A., LCDR, USN

5d. PROJECT NUMBER
2005-025

5e. TASK NUMBER

5f. WORK UNIT NUMBER

7. PERFORMING ORGANIZATION NAMES(S) AND ADDRESS(S)

Air Force Institute of Technology
Graduate School of Engineering and Management (AFIT/EN)
2950 Hobson Way
WPAFB OH 45433-7765

8. PERFORMING ORGANIZATION REPORT NUMBER

AFIT/GAE/ENY/07-J23

9. SPONSORING/MONITORING AGENCY NAME(S) AND ADDRESS(ES)

AFOSR/NL	AFRL/MLBCM	AFRL/MLBCM
Attn: Dr. Charles Y-C Lee	Attn: Greg Schoeppner	Attn: Richard Hall
875 Randolph St	2941 P Street	2941 P Street
Arlington, VA 22203-1954	WPAFB, OH, 45433,	WPAFB, OH, 45433,
Comm No: (703)696-7779	(937)255-9072	(937)255-9097

10. SPONSOR/MONITOR'S ACRONYM(S)

11. SPONSOR/MONITOR'S REPORT NUMBER(S)

12. DISTRIBUTION/AVAILABILITY STATEMENT

APPROVED FOR PUBLIC RELEASE; DISTRIBUTION UNLIMITED.

13. SUPPLEMENTARY NOTES

14. ABSTRACT

The creep behavior of IM7/BMI 5250-4 with fiber orientations of [±45] and [0/90] that were aged in air at 191ºC for up to 1000 hours was evaluated. The total weight loss during the aging process was also evaluated. Weight loss due to aging was 0.64% for the [0/90] fiber orientation and 0.72% for the [±45] fiber orientation.

Tensile tests to failure were conducted to establish tensile properties. The [0/90] specimens have a much higher stiffness and Ultimate Tensile Strength (UTS) values than the [±45] specimens. The tensile tests of the aged specimens revealed that the Ultimate Tensile Strength of the composite decreased and the modulus increased with increasing prior aging time.

Creep tests were conducted at 191ºC. The creep tests were of 100 hour duration and were followed by unloading to zero stress and 60 hours of recovery at zero stress.

15. SUBJECT TERMS

Composite, IM7/BMI 5250-4, creep, recovery, prior aging history

16. SECURITY CLASSIFICATION OF:			**17. LIMITATION OF ABSTRACT**	**18. NUMBER OF PAGES**	**19a. NAME OF RESPONSIBLE PERSON**
REPORT	**ABSTRACT**	**c. THIS PAGE**			Dr. Marina B. Ruggles-Wrenn
U	**U**	**U**	**UU**	109	**19b. TELEPHONE NUMBER** *(Include area code)* 785-3636, ext 4641; e-mail: @afit.edu